ACS OMEGA

Open Access

http://pubs.acs.org/journal/acsodf

Article

Design Characteristics of a Neoteric, Superhydrophilic, Mechanically Robust Hydrogel Engineered To Limit Fouling in the Ocular Environment

Onyinye J. Uwaezuoke, Pradeep Kumar, Lisa C. du Toit, Naseer Ally, and Yahya E. Choonara*

Cite This: *ACS Omega* 2024, 9, 31410−31426

Read Online

ACCESS | Metrics & More | Article Recommendations | Supporting Information

ABSTRACT: Current challenges with ocular drug delivery and the chronic nature of many ocular ailments render the use of traditional ocular devices for additional drug delivery purposes very attractive. To achieve this feat, there is the need to develop biomaterials that are biocompatible, mechanically robust for ocular applications, highly transparent (depending on the targeted ocular device), and with ultralow protein adhesion potential (the primary step in processes that lead to fouling and potential device failure). Herein is reported the facile synthesis of a novel, highly transparent, mechanically robust, nontoxic, bulk functionalized hydrogel with characteristics suited to scalable fabrication of ocular implantable and nonimplantable devices. Synergistic superhydrophilicity between methacrylated poly(vinyl alcohol) (PVAGMA) and zwitterionic sulfobetaine methacrylate was exploited to obtain a superhydrophilic polymer conjugate through facile photoinitiated cross-linking polymerization. Proton nuclear magnetic resonance (^{1}H NMR), attenuated total reflectance-Fourier transform infrared spectroscopy (ATF-FTIR), X-ray powder diffraction (XRD), thermogravimetric analysis (TGA), and differential scanning calorimetry (DSC) were used to confirm the synthesis and establish the physicochemical parameters for both the starting materials, the conjugated polymer, and the hydrogels. Cytotoxicity and cell adhesion potential evaluated in primary human retinal epithelial cells showed no toxicity or adhesion of the ocular cells. Biofilm adhesion studies in *Escherichia coli* and *Staphylococcus aureus* showed over 85% reduction in biofilm adhesion for the best-modified polymer compared to the unconjugated PVAGMA, highlighting its antifouling potential.

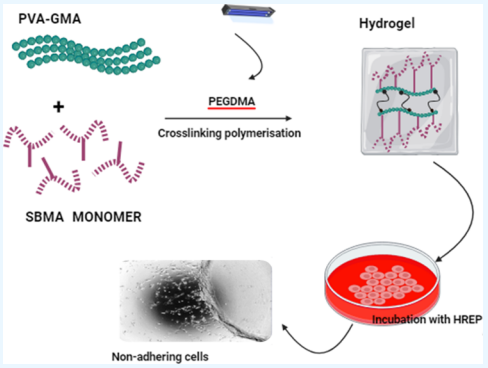

INTRODUCTION

Delivery of therapeutics to the eye continues to be challenging due to not only the anatomical and physiological barriers encountered by delivery systems to the eye but also due to the physicochemical nature of emerging new chemical entities used to treat ocular maladies.[1] Compounding these challenges is the skewing of the patient population requiring chronic therapeutic management of ocular conditions toward the aged due to improved life expectancy. Biomaterials are therefore increasingly being positioned to tackle this task in terms of maintaining the stability, presence, and deliverability of the included therapeutics over an extended period of time from a single implant application. Derived from these challenges, contemporary drug delivery to the ocular space is moving toward the use of traditional devices such as punctal plugs, contact lenses, intraocular lenses, etc. as drug delivery tools.[1] Such implants must, in addition, be able to limit the adsorption of proteins from body fluid that occurs ubiquitously with most biomaterials when placed in proximity to body fluids, as this may lead to fouling, biofilm formation, and ultimate implant failure.

Key characteristics required of ocular biomaterials are dependent on the specific ocular application. A biomaterial to be applied as a scleral or contact lens is required to be transparent, mechanically robust, nontoxic, biocompatible, and highly oxygen permeable with excellent wettability that limits fouling. Implanted biomaterials such as orbital implants, glaucoma drainage devices, and drug delivery inserts are additionally required to minimize the foreign body reaction and inflammation on application.[2,3] Wettability, which is often measured via the contact angle, has been used to evaluate propensity to limit tear film deposits and protein adsorption.[2]

Zwitterionic polymers possessing both cations and anions in their molecular backbone structure are an emerging alternative to the traditional use of poly(ethylene glycol) for improving hydrophilicity and limiting protein adhesion in biomaterials.

Received: January 8, 2024
Revised: April 22, 2024
Accepted: May 20, 2024
Published: July 9, 2024

Scheme 1. Synthesis of the PVAGMA Polymer

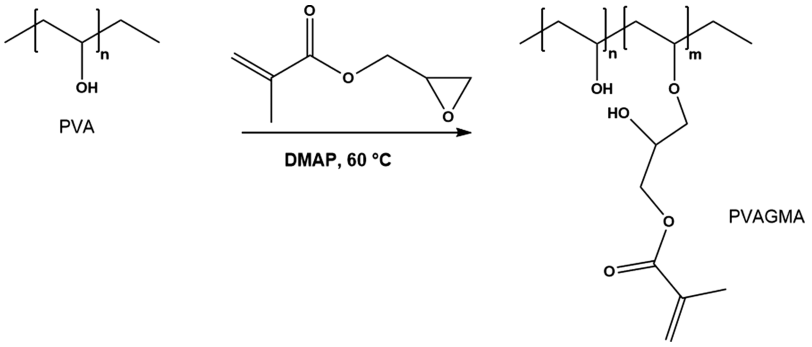

This is followed by the connection of the protein-resistant activity of phosphorylcholine to its zwitterionic structure.[4] The close structural resemblance of zwitterionics to naturally occurring molecules (for example, sulfobetaine methacrylate to 2-aminoethanesulfonic acid (taurine) which is a naturally occurring amino acid component of human muscular tissues), the superhydrophilicity of zwitterionics, their biocompatibility, and the additional potential to serve as ligands for conjugating drug molecules through the free carboxylic group, as is in the case of carboxybetaine methacrylate, render them appealing. Since then, several studies employing zwitterionic polymers such as sulfobetaine methacrylate (SBMA) and carboxybetaine methacrylate as a surface coating on a mechanically robust base material for imparting protein resistance have been undertaken.[5] Some of these studies in which zwitterionic polymers were used in combination with other polymers also identified the softening effect of the zwitterionic polymer.[6] As a panacea to the major drawback to the stand-alone use of zwitterionics in medical devices and implants (limited mechanical robustness), Carr and co-workers synthesized and used a cross-linker with a structural resemblance to the zwitterionic.[7] Their work showed an improvement in the mechanical properties of hydrogels formed using the new zwitterionic cross-linker over the hydrogels prepared with the traditional methylene bis(acrylamide) (MBAA). This improvement was ascribed to the improved solubility of the synthesized zwitterionic cross-linker at all concentrations over that of pure MBAA.[7] Unfortunately, the added synthesis of the zwitterionic cross-linker is complex and adds to the overall cost of the hydrogels. Even though surface modification with other hydrophilic polymers and zwitterions has yielded protein-resistant biomaterials, the durability of these coatings is still a concern particularly due to the dynamic nature of the environment for specific ocular applications.[1]

Poly(vinyl alcohol) (PVA) is another polymer that has been used in surface modification of commercially available contact lenses where its hydrophilicity was exploited to impart protein resistance. Other investigators had reported the potential use of PVA as a stand-alone hydrogel for ocular application with appropriate mechanical strength.[8] The hydrophilicity and high swelling of PVA hydrogels have also great implications for its mechanical strength; hence, Tummala and co-workers[9] (following the method of Kita and co-workers[8]) explored its use in a contact lens but with reinforcement with carboxylated nanocellulose whiskers. Another drawback to the use of PVA in ocular applications, particularly for contact lens applications, is its lack of adhesiveness; hence, if used in an application such as a lens or patch, it may not remain on the ocular surface. Additionally, traditional methods of cross-linking PVA involving the physical process of freeze−thaw cycles and the chemical cross-linking using glutaraldehyde are both time-consuming and tedious and may have implications for safety. Methacrylation of PVA enables the photopolymerization process, which has been proposed as a better method for the fabrication of hydrogels for biomedical applications in view of the shorter time periods of exposure, amenability to room temperature operation, and the availability of biocompatible photoinitiators.[10,11]

Herein, we report the fabrication of a hydrogel for potential ocular application using two highly hydrophilic polymers, PVA and SBMA. A synergistic potentiation in the hydrophilicity of the expected hydrogel was hypothesized ab initio with a view to possibly limiting protein adhesion to the surface of the hydrogel as a result of the expected maximized hydrophilicity. With the expected possible mechanical deficit under consideration, this work set out to exploit the possible synergy of two hydrophilic polymers, poly(vinyl alcohol) (PVA) and sulfobetaine methacrylate (SBMA), in developing a protein-resistant biopolymer for ocular application. PVA was first methacrylated to render it photo-cross-linkable while improving its adhesiveness. In a facile, one-step process, the SBMA monomer was grafted onto poly(vinyl alcohol) methacrylate by a photoinitiated cross-linking polymerization. A concentration-dependent improvement in transparency, protein adhesion resistance, antibiofouling potential, and serendipitously, mechanical strength from an apparently mechanical strength-deficient polymer, SBMA, was observed. The developed biomaterial has the potential to relegate the traditional use of surface coatings that deteriorate readily and lower the cost of the use of additional antimicrobials to limit biofilm adhesion.

EXPERIMENTAL SECTION

Materials. Poly(vinyl alcohol) (PVA) (Mw 89,000−98,000 m/mol, 98+% hydrolyzed), Irgacure 1929, polyethylene glycol dimethacrylate (PEGDMA) Average Mn 750, 1,3-propane sultone, dimethyl aminoethyl methacrylate (DMAEMA), dimethyl sulfoxide (DMSO), glycidyl methacrylate (GMA), and dimethyl aminopyridine (DMAP) were all purchased from Sigma-Aldrich (St Louis, MO, USA). All other reagents were of the highest laboratory standards and used as received.

Synthesis of Sulfobetaine Methacrylate. Sulfobetaine methacrylate monomer was synthesized following a previously reported method in which equimolar concentrations of 1,3-propane sultone and DMAEMA were reacted together.[12] Briefly, a solution of propane sultone in 50 mL of acetone was introduced to a round-bottomed flask to which a dropping

https://doi.org/10.1021/acsomega.4c00228
ACS Omega 2024, 9, 31410−31426

funnel was attached and placed on a magnetic stirrer set at 40 rpm. A solution of DMAEMA (passed through basic alumina to remove the inhibitor) was introduced into the dropping funnel and allowed to drop into the round-bottom flask over a period of 1 h. The reaction flask was maintained in the dark for 48 h for the reaction to proceed to completion. Thereafter, the resulting white precipitate was collected by filtration and purified by recrystallization from an acetone/methanol solvent mixture.

Synthesis of the GMA-Modified PVA (PVA-GMA). PVA-GMA was prepared as illustrated in Scheme 1. Poly(vinyl alcohol) solution (10% w/v) was prepared in anhydrous DMSO in a two-arm round-bottom following a modified method from previous reports.[13] DMAP (0.22 g) and 0.6 mL of GMA were introduced into the flask, which was stirred under nitrogen at 60 °C for 1 h. PVA-GMA was recovered from the reaction mixture using a large excess of acetone. The resulting white precipitate was washed twice with acetone and dried under vacuum for 48 h. The concentration of GMA was varied to achieve different degrees of methacrylation.

Zwitterionization and Photoinitiated Cross-Linking Copolymerization of PVAGMA and SBMA. Required quantities of PVAGMA and SBMA were dissolved in ∼6 mL of mixed solvent system containing 80% DMSO in deionized water. The ratio of PVAGMA to SBMA varied from 1:0 to 1:0.25. PEGDMA (varied between 3 and 5% w/w and Irgacure 1929 (1% w/w) were added to the polymer solution and stirred. Air bubbles were removed by ultrasonication in a bath sonicator at 27 °C for 5 min. Cross-linking polymerization was subsequently carried out in a UV chamber powered by a 365 nm light for 10 min. The resulting hydrogels were immersed in an excess amount of deionized water over 72 h with daily water changes for rehydration and elimination of unreacted components. Different characteristics of the formed hydrogel were optimized by varying different components, namely, PVAGMA and SBMA. A general nomenclature was used to name each hydrogel formulation based on the two constituent polymers, PVAGMA and SBMA, coded PM and SM, respectively, and the numbers following immediately after each component representing the percentage content of that polymer relative to the second polymer. As an example, PM90-SM10 codes for a formulation in which the ratio of the PVGMA: SBMA is 90:10.

Characterization of the PVA-GMA Base Material and Sample Hydrogels. Attenuated total reflectance-Fourier transform infrared spectroscopy to determine the molecular transitions within the pristine and modified components was performed using a PerkinElmer Spectrum 2000 ATR-FTIR spectrometer (PerkinElmer 100, Llantrisant, Wales, U.K.) fitted with a single-reflection diamond MIRTGS detector. Analysis was obtained in the 4000−650 cm^{-1} range after 60 scans. Proton nuclear magnetic resonance (^1H NMR) spectra were obtained at 90 °C in deuterated DMSO on a BRUKE Avance 111 400 MHz spectrometer (Massachusetts, USA). Thermal properties and thermogravimetric analysis were undertaken on the (Mettler Toledo, DSC, STARe System, Swchwerzenback, ZH, Switzerland) and (PerkinElmer, TGA 4000, Llantrisant, U.K.) apparatuses, respectively. For DSC measurements, between 3 and 10 mg of the sample to be analyzed was sealed in aluminum crucibles and heated over a temperature range of 20 to 300 °C at a heating rate of 10 °C/min under a N2 atm in Mettler Toledo, DSC, STARe System, Swchwerzenback, ZH, Switzerland. DSC curves were obtained as plots of the heat flow against temperature. For TGA, Samples were heated at a rate of 10 °C/min from 30 to 900 °C under continuous nitrogen purging. X-ray powder diffraction (XRD) to delineate the crystallinity of the individual modified and unmodified components of the hydrogel and the hydrogel was determined on a benchtop diffractometer (Rigaku Miniflex 600, Rigaku Corporation, Matsubara-cho, Akishima-shi, and Tokyo, Japan) using CuKα radiation at 40 kV and 15 mA. The diffractograms were obtained at a scanning 2θ range between 5 to 90 deg at a scan rate of 10 degrees per minute. The scan step of 0.02 °C was used throughout. The surface area and porosity of the dried hydrogel sample were measured using the BET and BJH principles of the Porositometric analyzer (Micromeritics ASAP 2020, Norcross, GA, USA). A minimum of 100 mg of a sample of the dried hydrogel was initially degassed and subsequently subjected to analysis at an evacuation rate of 50 Hg/s and a temperature ramp of 10 °C per minute. The targeted temperature was 115 °C which was maintained for 900 min until completion of the analysis. The morphology of the hydrogels was studied with field emission scanning electron microscopy (SEM) of ZEISS Sigma 300 VP with a ZEISS "smart SEM" software (field emission scanning electron microscope, FEI, Orlando, Florida, USA). For this analysis, dried hydrogel samples were fractured in liquid nitrogen and mounted on aluminum stubs to view the planar and cross sections of each hydrogel, which was coated with palladium/gold at an accelerating voltage from 10 to 15 kV.

Mechanical and Viscoelasticity Profiling. The mechanical characteristics of sample hydrogels swollen in artificial tear fluid were studied using the compression mode of the texture analyzer (TA. XT plus texture analyzer, Stable Microsystems, Surrey, U.K.) at room temperature fitted with the compression platen probe (0.5r) at different strain percent. The diameter and height of a cylindrical sample punched with a 6 mm skin biopsy punch were measured using (Kraft, DV150GW, Schoellerstr Düren, German). Each sample disc was first subjected to 10 compression cycles at a 40% strain and afterward compressed to failure at 70% strain using an auto trigger force of 0.001 kG at room temperature. The shear storage modulus, Shear loss modulus, compressive modulus, and tan d of equilibrium swollen hydrogel discs were determined on an ElastoSensBio (Rheolution instruments, Canada). A single measurement with a temperature profile from 25 to 37 °C was undertaken to determine viscoelastic properties between the handling temperature and the body temperature. The temperature was set to 5 °C.

Determination of Equilibrium Water Uptake (EWU). To determine the percent swelling of the hydrogel, we determined the initial weight of an equilibrium swollen hydrogel was determined. Subsequently, the hydrogel was dried in a vacuum oven set at 90 °C to a constant weight. The percent swelling is subsequently determined using eq 1:

$$\%\text{Water uptake} = (\text{Weight of swollen hydrogel} - \text{Weight of dried hydrogel}) / (\text{Weight of dried hydrogel}) \times 100 \quad (1)$$

Determination of the Water Contact Angle Measurement. The water contact angle is usually used as an indication of the hydrophilicity of any material and, by extension, its

https://doi.org/10.1021/acsomega.4c00228
ACS Omega 2024, 9, 31410−31426

protein resistance potential. The water contact angle of a sessile water drop of distilled water on an equilibrium swollen hydrogel was determined on a Data Physics Instruments contact angle goniometer. Each sample was wiped with filter paper to remove excess water from the surface of the hydrogel and mounted on a stage. Distilled water (1 μL) was delivered on the surface using a Hamilton syringe at a dosing rate of 1 μL s^{-1}. The digital picture of the stabilized droplet was subsequently recorded using the camera software, while the contact angle was measured using SCA202 version 4.1.12 build software. The procedure was repeated at three different points in each sample.

In Vitro Assessment of Protein Adhesion to the Hydrogel Samples. The amount of protein adsorbed onto the hydrogel was quantified using a Micro BCA protein assay kit. For the adsorption study, discs were punched out of the hydrogel, and the dimensions were noted. For each hydrogel formulation, 3 such discs were punched and immersed in a protein solution and thereafter incubated in an orbital shaker set at 37 °C for 1 h. The artificial tear fluid (ATF) containing a mixture of proteins was prepared by dissolving lysozyme, mucin, bovine serum albumin (BSA), and calcium chloride in phosphate-buffered saline (PBS) pH 7.4. After the incubation, the discs were washed in PBS 3 times, and subsequently, a 1% sodium dodecyl sulfate solution was used to detach the protein adsorbed to each of the discs. The amount of protein adsorbed to each disc was measured by using the Implen Nano-Photometer according to the protocol of the Micro BCA protein assay kit.

Cytotoxicity Evaluation of the Hydrogel Extract Using a 3-[4,5-Dimethylthiazol-2-yl]-2,5-diphenyltetrazolium Bromide (MTT) Assay. MTT assay to determine the cytotoxicity of extractables from the hydrogel was carried out using 3T3 fibroblast and an ocular cell line, human retinal epithelial primary (HREP) cell lines. RPMI medium supplemented with 10% fetal bovine serum (FBS) and 1% penicillin/streptomycin was used as the culture medium for 3T3 cells, while HREP cells were grown in DMEM: Ham's F-12 (50:50) supplemented with 10% FBS and 1% penicillin/streptomycin. The cells were grown to 80 to 90% (about 48 h incubation) confluence in an incubator set at a temperature of 37 °C with 5% CO_2. Thereafter, the cells were detached using about 2 mL of 1% trypsin. The cell suspension (90 μL) was thereafter seeded per well in two 96-well plates from a cell suspension at a cell density of 30,000 cells/mL for 3T3 cells and 40,000 cells/mL for HREP cells. The plates were further incubated for 24 h, and thereafter, each well was treated with 10 μL of the extract from the hydrogel prepared by incubating each hydrogel formulation in ATF at 37 °C for 7 days. After 24 and 48 h, respectively, each well plate was treated with 10 μL of (3-[4,5- dimethylthiazol-2-yl]-2,5-diphenyltetrazolium bromide) (MTT) at a final concentration of 5 mg/mL. Each plate was further incubated for 4 h in a humidified atmosphere at 37 °C and 5−6% CO_2. The solubilization reagent (100 μL) was then added and the plate was allowed to stand overnight in the incubator. The absorbance of the developed purple formazan crystals was then read in a VX3 microplate reader at 570 nm. The percent viability of the cells was subsequently calculated using eq 2.

$$\%\text{Viability} = (\text{Absorbance of treated well} - \text{absorbance of blank}) / (\text{Absorbance of control} - \text{absorbance of blank}) \times 100 \quad (2)$$

ATF was used as the negative control; 5 fluorouracil was used as the positive control, and untreated wells were used as the blank.

Determination of Cell Adhesion Using HREP. Cell adhesion studies were undertaken to determine the proliferation capacity of human retinal epithelial cells on the prepared hydrogels. Hydrogel discs (4 × 0.75 mm) were punched in triplicate from each pristine PVGMA hydrogel (PM100-SM0), with 20 (PM80-SM20) and 33% SBMA (PM67-SM33). HREP cells were revived and grown to a 70% confluence in a DMEM: Ham 12 (50:50) medium was supplemented with 10% fetal bovine serum and 1% penicillin strep. Subsequently, the equilibrium swollen discs were each inserted into a well in a 48-well plate. HREP cells (300 μL) were seeded at a density of 40,000 cells/mL on top of the hydrogel discs in the well plate and incubated at 37 °C and 5% CO_2 for 4 h. Digital images were captured at both the center of the hydrogel and the boundary between the hydrogel and the well plate. To confirm if the few cells observed on the hydrogel were attached to it or on the well plate under the hydrogel, the gels were washed with sterile PBS and fixed with 4% formalin. 4′,6-Diamidino-2-phenylindole. DAPI was subsequently used to stain the nuclei of any cells attached to the hydrogels and visualized with a confocal laser microscope.

Assessment of Biofouling Potential of Hydrogels. Two bacterial cell lines, a Gram-positive (*Staphylococcus aureus*) and a Gram-negative (*Escherichia coli*) (ATCC25922), known for high contamination potential were used to assess the antibiofouling capacity of the as-modified hydrogels. Hydrogel discs measuring 4 × 0.75 mm were sterilized by autoclaving and inserted into a sterile suspension of each microbe previously cultured at 37 °C for 24 h in Luria−Bertani medium consisting of 1% w/w tryptone, 0.5% w/w yeast extract, 1% w/w NaCl, and 1.5% w/w agar in sterile deionized water. The hydrogel disc in the bacterial suspension was incubated at 37 °C for a further 24 h. The hydrogel discs were removed thereafter, washed 3 times with sterile Dulbecco PBS to remove unattached bacteria, and the bacteria adhering to the disc was detached with a rubber policeman and counted to determine the number of colony-forming units, (CFU mL^{-1}).

Statistical Analysis. Results are reported as the mean ± the standard deviation of triplicate readings. Where necessary, comparisons between means are undertaken using the student *t*-test and one-way analysis of variance using Microsoft Excel 2016 (Microsoft Corp, WA, USA) and GraphPad by Dotmatics (Boston, Massachusetts).

RESULTS AND DISCUSSION

Synthesis and Spectral Characterization of Pristine and Zwitterionic PVAGMA and Their Hydrogels. PVAGMA was synthesized by the grafting of a methacrylic moiety to PVA via the ring-opening reaction of GMA in the presence of PVA. The SBMA was added as a monomer in the hydrogel-forming mixture with the expectation that polymerization would take place simultaneously with the cross-linking.

https://doi.org/10.1021/acsomega.4c00228
ACS Omega 2024, 9, 31410−31426

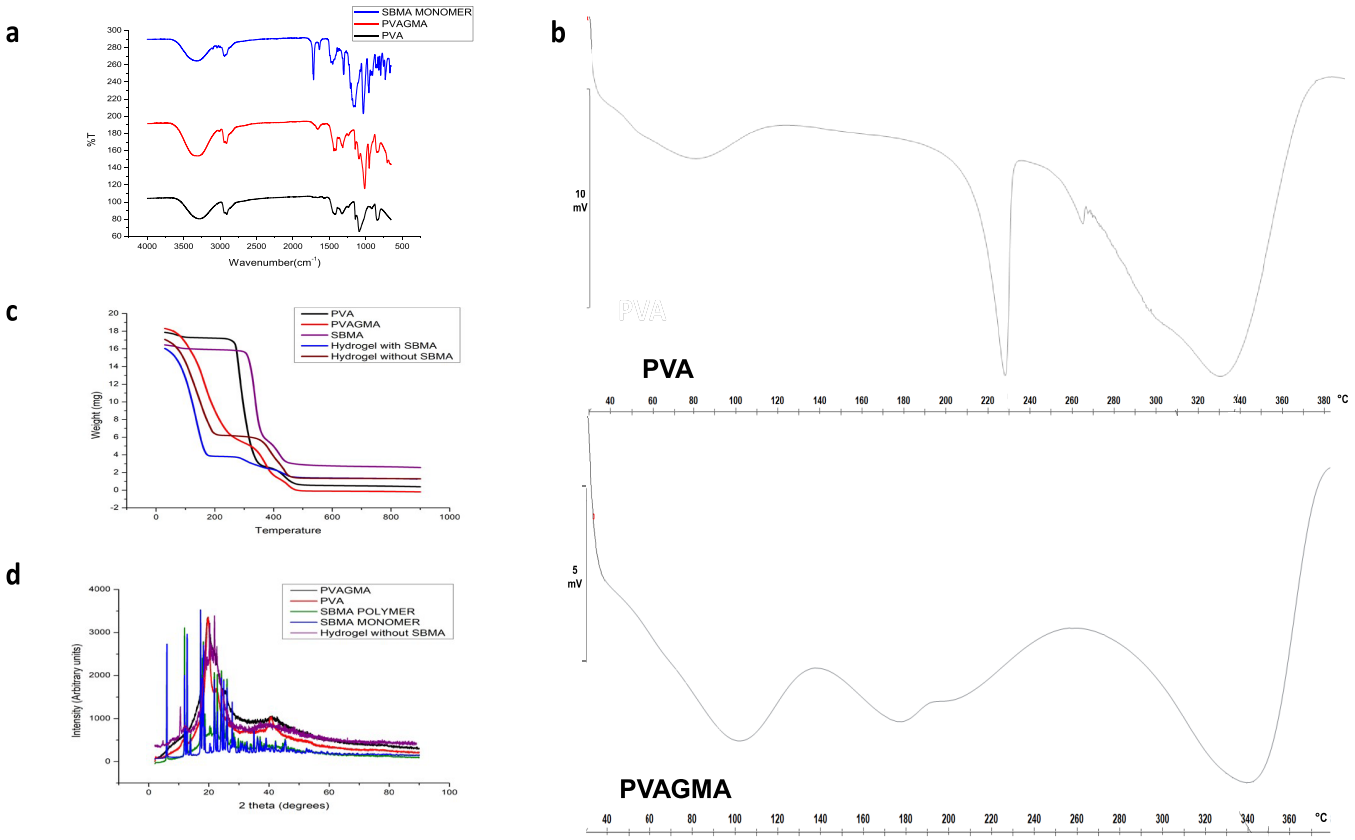

Figure 1. Spectral characterization of (a) PVA, PVAGMA, and SBMA via FTIR, (b) PVA and PVAGMA via DSC, (c) PVA, PVAGMA, SBMA, and hydrogel variants via TGA, and (d) PVA, PVAGMA, SBMA, and hydrogel variants via XRD.

Table 1. Wavenumber Assignments for PVA and PVAGMA

assignments	PVA absorption wavenumber (cm^{-1})[14]	PVA absorption wavenumber (cm^{-1})[14]	PVAGMA absorption wavenumber (cm^{-1})[14]
OH stretching	3340	3283	3319
CH_3 stretching			3001
CH_2 stretching	2942	2907	2913
C═O from ester			1708
C═C stretching			1642
CH_2 bending	1430	1420	1452
C−O−C stretching	1141	1142	
C═O stretching	1096	1087	1093
C−C stretching	850	848	845

ATR-FTIR is an excellent tool for the delineation of the vibrational patterns of dipole moments of compounds that result from infrared absorption or transmittance and was used in analyzing the molecular transitions occurring at every step of the synthesis. The analysis shown in Figure 1a confirmed the molecular transitions incurred by the methacrylation of PVA. Table 1 summarizes the various peaks that appeared in modified PVA and their absorption wavenumbers. The characteristic C═O stretching of the methacrylates was evident at 1708.15 cm^{-1} while the C═C stretch was observed at 1642.96 cm^{-1}. Previous studies had assigned the OH stretch of PVA to the peak at 3280 cm^{-1}, and the $-CH_2$ asymmetric stretch to the peak at 2917 cm^{-1}.[1] The peak at 1690 cm^{-1} is assigned to the C═O. The CH bending vibration is noted at 1425 cm^{-1}; the C−H deformation vibration is evident at 1324 cm^{-1}, the C−O stretching of the acetyl group is at 1081 cm^{-1}, and the C−C stretching at 839 cm^{-1}.[4]

Zhou and co-workers, in their work in which SBMA was grafted to chitosan, reported stretching vibrations of $-CH_2$, −C═O, and −-S═O bonds resulting from SBMA grafting at 2934, 1750, and 1150 cm^{-1}.[5] Likewise, Lalani and Liu assigned the FTIR peaks appearing at 1160 and 1032 cm^{-1} to the asymmetric and symmetric S═O of the sulfonate group, respectively, while assigning the peak at 1480 cm^{-1} to the quaternary ammonium bond in the poly sulfobetaine spectrum.[6] The peaks appearing at 1161 and 1034 cm^{-1} in the SBMA monomer spectrum in Figure 1a are assigned to the asymmetric and the symmetric −S═O bonds, respectively, of the sulfonate group, while the peak at 1418 cm^{-1} is assigned to the quaternary ammonium group.

In Figure 1a, the FTIR spectra of the lyophilized PVAGMA hydrogels copolymerized with 20 (PM80-SM20) and 33% w/w SBMA (PM67-SM33) and hydrogel composed of PVAGMA alone (PM100-SM0) are shown. The peaks appearing in the range 2943−3043 cm^{-1} representing the CH_2 groups and

https://doi.org/10.1021/acsomega.4c00228
ACS Omega 2024, 9, 31410−31426

methyl groups of the methacrylate group in the SBMA monomer disappeared in the hydrogels in which SBMA had been copolymerized with PVAGMA, as observed for PM80-SM20 and PM67-SM33. Additionally, the appearance of the peak at 1170 cm^{-1} highlighted the presence of the stretching vibrations of S═O of the SBMA, thus confirming the copolymerization of SBMA with the PVAGMA hydrogel. The C═O band confirmed the presence of the ester group and was evident at 1708 and 1716−1722 cm^{-1} in the PVAGMA and SBMA spectra, respectively. The stretching vibrations that appeared at 2997 and 3001 cm^{-1} in the PVAGMA and SBMA spectra are due to the C−H stretching of the methacrylate group. In addition, the peak occurring at ∼1640 cm^{-1} confirmed the polymerization of methacrylates,[7] and the shift of the wavenumber and the intensity verified the polymerization of SBMA in the hydrogel.

The chemical shifts of the different protons occurring in PVA were analyzed via proton NMR undertaken in deuterated DMSO, and employed to further confirm the methacrylation of PVA, as shown in Figure S1. In addition, the effect of doubling the concentration of glycidyl methacrylate during the methacrylation of PVA was also corroborated using ^{1}H NMR. When compared with the ^{1}H NMR spectra of pristine PVA, that of methacrylated PVA (Figure S2), singlet proton signals appeared at the chemical shifts of 5.65 and 6.0 ppm and represent the vinyl protons from GMA. The group of protons occurring at the chemical shift of 1.5 ppm is assigned to the CH_2 of the PVA backbone. These protons are a combination of doublets and triplets, arising from the varied nature of their chemical environment. The doublet signal occurs downfield at a chemical shift of 3.9 ppm, which has been assigned to the CH group attached to the oxygen atom of the PVA. The degree of methacrylation (DM) is found by determination of the integral (peak area) of the peaks arising from the methacrylate group occurring at chemical shifts 5.65 and 6.0 ppm as a ratio to the integral of the methine protons of the PVA backbone occurring at chemicals shifts 4.2 to 4.3 ppm. By visual comparison of the NMR spectra of PVAGMA with a lower concentration of GMA (DM = 0.06) and that with higher GMA (DM = 0.12) as depicted in Figure S2, it is evident that these peaks representing chemical shifts at 5.65 and 6.0 ppm became more visible in the NMR spectra of the PVGMA prepared with a higher concentration of GMA thus showing a higher degree of substitution.

The thermal events that occurred when PVA and PVAGMA were subjected to heat flow in a DSC furnace are shown in Figure 1b. The glass transition temperature, T_g, and melting point of the PVA used in this work were determined at 80.81 and 208.08 °C respectively. Although this varied by 0.81 and 8.0 °C with that reported in the literature for reference samples,[8] other studies had shown glass transition temperatures of 85 °C[10] and 70 °C.[11] Strawhecker and Manias, additionally reported a melting point of 225 °C.[11] These differences have been attributed to the variability in the degree of crystallinity obtained from different batches of PVA, the degree of hydrolysis, and the determination technique or process. The melting temperature was associated with 91.26 J g^{1-} of energy, with an endothermic peak at 228.75 °C. The small shoulder occurring at 265.48 °C could be attributed to crystallization occurring very close to melting. Decomposition was noted from ∼344 °C. Methacrylation of PVA resulted in a polymer with a higher T_g of 99.22 °C, a melting endotherm of 153.7 °C, and a decomposition peak at 330.9 °C. Increasing the degree of methacrylation shifted the T_g and melting point even further. This differed greatly from 66.1 °C observed by Zhou and co-workers.[15] The difference is not surprising since the PVA used in their study was of different molecular weights and degrees of hydrolysis. In addition, the melting peaks of partially crystalline polymers depend on the distribution of crystallinities within the bulk of the polymer. Many other parameters such as the degree of methacrylation will also determine the T_g of the modified polymer. The thermogram of the SBMA monomer (Figure S3) did not show any glass transition temperature and reflects the crystalline nature of the monomer. Even for the SBMA polymer, Lalani and co-workers did not observe a glass transition temperature from the DSC of the SBMA polymers but rather observed a broad endothermic peak at 122, 137, and 150 °C depending on the molecular weight of the polymer.[6] In the DSC thermogram of the SBMA monomer shown in Figure S3, a melting endotherm appeared at 146.3 °C closely followed by a peak resembling that of cold crystallization at 157.61 °C. The decomposition temperature was observed at 326.17 °C. On the other hand, the DSC curve of a hydrogel sample containing SBMA (Figure S4) portrayed major thermal events at 71.36, 187.16, 261.34, and 258.5 °C corresponding to the T_g, melting point, and decomposition temperatures, respectively. The crystallinity of the SBMA monomer was not reflected in the hydrogel. This is proposedly because the SBMA monomer polymerized and cross-linked in the hydrogel as corroborated by the XRD results. The degree of crystallinity of the polymerized SBMA is lower than that of the monomer. Cross-linking polymerization led to the formation of amorphous areas. Fathi and co-workers observed the same effect while working with PVA xerogels. The physical cross-linking process involved in the xerogel formation caused a significant reduction in the melting endotherm attributed to the ordering effect which resulted in more closely packed crystals.[10]

The thermogravimetric analysis depicts the decomposition of substances under temperature. The decomposition of PVA will, usually, yield varied end products that may include alcohols, acetone, acetaldehyde, and water depending on the starting material.[10] Figure 1c shows two distinct degradation phases from the TGA of PVA. The weight derivative curve (Figure S5) shows a third phase at ∼77 °C that could represent the T_g of PVA since the weight loss associated with that phase is very minimal. The bulk of the decomposition occurred at around 277 °C, which closely corresponds to the temperature of the shoulder observed in the DSC curve. The onset temperature of the final decomposition phase was ∼350 °C peaking at 434 °C. The TGA curve of PVAGMA was very different from that of PVA with the weight derivative curve (Figure S5) showing 3 peaks in which the weight loss was more evenly distributed when compared to that of PVA. The first phase of the weight loss (over 60%) occurred at a higher peak temperature (compared to PVA) of 164 °C, while the second phase (involving 28% weight loss) occurred at a peak temperature of 367 °C. The last phase of decomposition of the PVAGMA peaked at ∼450 °C. This highlights the temperature-stabilizing effect of methacrylation on PVA. The TGA and weight derivative curves of the hydrogels prepared with and without SBMA were obtained. The curve differed from that of uncross-linked PVAGMA in terms of intensity of the weight derivative peaks and a slight shift in the corresponding peak temperatures. In addition, the peaks of the weight derivative curve depicting the second and the third phases of

https://doi.org/10.1021/acsomega.4c00228
ACS Omega 2024, 9, 31410−31426

the decomposition are not clearly separated at the base. This signifies that the third phase of the decomposition started, while the second phase was yet to end. The peak temperatures for these phases are 148, 388, and 437 °C. These differences may have resulted from the higher water content of the hydrogels. The TGA curve of the hydrogel containing SBMA differed visibly from that without SBMA. The intensities of the second and third phases of the TGA weight derivative curves were very low. The peaks for the thermal events occurred at 140, 298, and 358 °C.

The contributions and presence of both crystalline and amorphous regions in various samples were studied by using XRD powder diffraction. The diffractograms of the PVA, PVAGMA, SBMA (polymer and monomer), and a hydrogel sample with SBMA are shown in Figure 1d. PVA, being semicrystalline, exhibited peaks at 2θ = 19.8° and 40.4° close to the 20° and 40° values previously reported.[16] An additional peak that disappeared in the PVAGMA diffractogram was recorded for PVA at 2θ = 11° and further confirms modifications to the pristine PVA.

In addition, the visible reduction in the intensities of the peaks occurring at 2θ = 19.8° and 40.4° in PVA from 6641 and 2085 arbitrary units to 3378 and 1057 arbitrary units in the PVAGMA, respectively, represents the introduction of disordered amorphous regions or cavities in the PVAGMA. The exact size of the reduction, as shown in Figure S6, is represented by an increase in the value of the full width at half-maximum (FWHM) calculated for PVA and PVAGMA from 5.864 to 8.417 nm, respectively.

FWHM varies inversely with the crystallite size as shown by Scherrer's equation.[17] This indicates that either the methacrylation of PVA led to the smaller crystallite sizes within the PVAGMA or the creation of a more ordered packing of the crystals led to free spaces within the PVAGMA structure. Zhang and colleagues made a similar observation for a composite hydrogel of PVAGMA and cellulose nanofibrils (CNF). They reported that inclusion of CNF affected the crystallinity of PVAGMA.[13] They reported only one peak appearing at 2θ = 19.4 in the XRD of PVAGMA which they attributed as arising from the orthorhombic lattice of semicrystalline PVA. In like manner, the XRD curves for both polymerized SBMA and the SBMA monomer were compared to enable the elucidation of the contributions of SBMA in the resultant hydrogel. The peaks for both the monomer and polymer of SBMA occurred at the same 2θ positions but differed in intensities. Since the peak intensities represent the magnitude of the contributions of each crystal to the crystallinity of that phase,[18] it then highlights that the crystallinity of SBMA reduces with polymerization. In the synthesis of the hydrogel, SBMA was added in a monomeric form. The resulting XRD confirms the disappearance of the crystallite peaks that were so prominent for the SBMA monomer but with reduced intensity in the SBMA polymer diffractogram. Table 2 outlines the full width at half-maximum (fwhm) for the first 5 peaks in SBMA monomer, SBMA polymer, and a hydrogel sample, PM89-SM11. The hydrogel showed a single peak of very low intensity at 2θ = 10.5 and fwhm of 6.909 nm. Peaks 2 to 5 in the PM100-SM0 hydrogel originated as a single broad peak at 2θ = 18.78° and only split at the top into 4 different peaks which are recorded in Table 2. This represents a further increase in the amorphous regions in the hydrogel.

Table 2. FWHM for the Component Peaks in SBMA Monomer, SBMA Polymer, PVAGMA, and PM89-SM11

	full width at half-maximum [nm]			
2θ [deg]	SBMA monomer	SBMA polymer	hydrogel with SBMA	PVAGMA
6.11	1.342	13.855		
10.52			6.909	
11.57	1.295	1.076		
12.81	0.151	12.318		
17.25	0.223			
17.86	0.196	17.472		
18.20	0.178	33.800		
18.78			3.762	
20.33			38.919	8.417
21.93			5.382	
22.71			33.370	

Mechanical and Viscoelastic Properties of Hydrogels.

The mechanical robustness of hydrogels is an important attribute that dictates, to a large extent, their usability for each application. Hydrogels, by virtue of their high water content, are usually soft materials. Their elastomeric inclination makes them attractive alternatives in many soft tissue applications. Despite their soft nature, hydrogels are required to exhibit a measure of strength that makes handling possible. In certain ocular applications, such as the contact lens and scleral patch, the hydrogel should be strong enough to withstand shearing brought about by blinking in addition to being handled during insertion by the patient. This may be a big challenge considering that the water content, which varies inversely with the mechanical strength, is very important, as it contributes heavily to the oxygen permeability in such applications. All prior studies involving UV-cross-linkable PVAGMA hydrogels (where not used alone) had involved the use of materials such as cellulose nanofibrils,[13] hydroxyapatite,[15] and chondroitin sulfate,[19] aimed at reinforcing the mechanical robustness of PVAGMA hydrogels. In other studies, it was a symbiotic approach by which, for instance, the mechanical robustness of polysulfobetaine methacrylate was improved by grafting with polymers such as chitosan while chitosan's ability to resist protein adsorption was improved.[5] Rarely has polysulfobetaine methacrylate been used alone, mainly because of its deficit in mechanical robustness. Only one such study was found (within the limits of literature available so far) in which electrospun fibers from polysulfobetaine methacrylate were explored for wound healing applications.[6] This is not surprising, as the mechanical strength demands on hydrogels for wound healing applications are minimal. In a similar study involving sulfobetaine acrylamide, nanoclay was employed as a reinforcing cross-linker.[20] Representative graphs of the results obtained from the compressive stress−strain cycles (a−c) and of select hydrogel samples are shown in Figure 2, while results of the compression to failure are presented in Table 3. Compressive stress−strain curves were obtained in cyclic mode for 10 cycles on each sample before being compressed to failure (i.e., the strain was increased until we attained the strain level required to compress the sample to failure). A 40% strain was used for each compressive cycle while a 70% strain was used for compression to failure. In some of the samples, a strain higher than 80% was required to deform the samples to failure, while the sample without SBMA failed with a 50% strain.

https://doi.org/10.1021/acsomega.4c00228
ACS Omega 2024, 9, 31410−31426

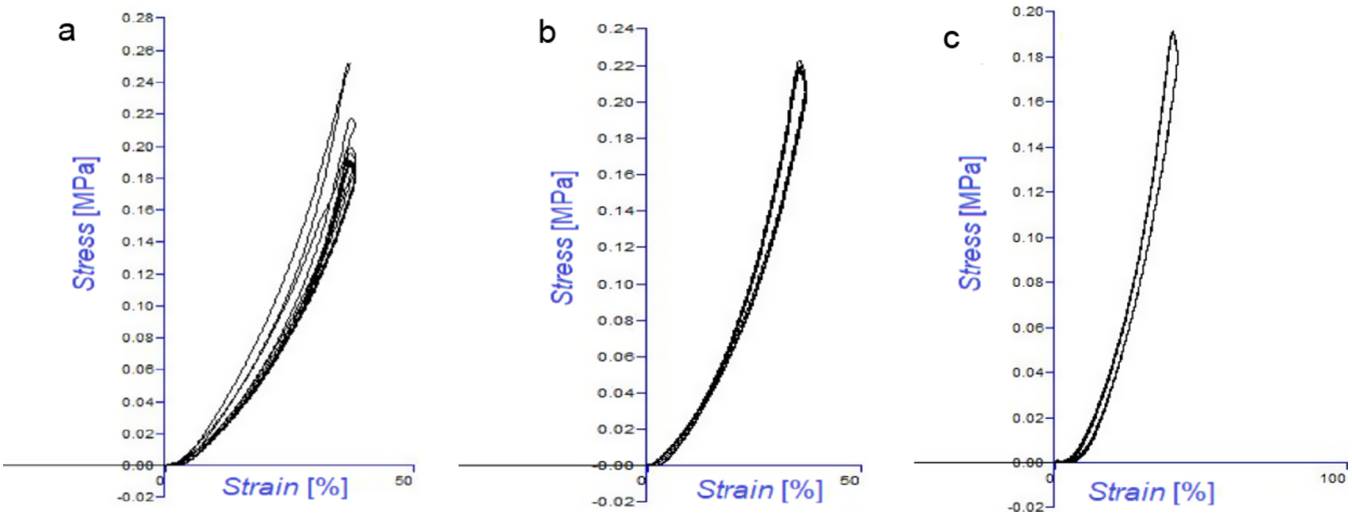

Figure 2. Compression stress−strain curves for 10 cycles at 40% strain for (a) PM100-SM0, (b) PM88-SM12, and (c) PM67-SM33.

Table 3. Mechanical Parameters of the Hydrogel Samples Compressed to Failure at 70% Strain

sample name	SBMA content (% relative to PVAGMA)	Young's modulus (MPa%)	peak stress (MPa)	compressive strength (area under the curve) (MPa%)
PM100-SM0[a]	0	0.015[a] ± 0.0013	0.1992 ± 0.0006	7.63 ± 0.0004
PM67-SM33	33	0.015 ± 0.0002	0.46 ± 0.0015	7.37 ± 0.0006
PM88-SM12	12	0.013 ± 0.0033		3.12 ± 0.0019
PM80-SM20	20	0.020 ± 0.0001	1.224 ± 0.0009	21.66 ± 0.0038

[a]Determined at 50% strain.

Compression to failure was required to determine the strength of the hydrogels. All the samples (selected results shown) withstood 10 compressive cycles. The graph appeared as that of a single cycle with no shifts in going from one cycle to the other for samples containing SBMA. This represents the stability of the hydrogels and their ability to recover uniformly when subjected to a shearing stress of such magnitude. In addition, the size of the hysteresis represents the energy dissipated by the hydrogel in the form of heat while unloading.

Hard materials are known to have minimal hysteresis, while elastomers with high elongation potential exhibit large hysteresis. A visual comparative analysis of the graphs in Figure 2a−c for samples containing 0 SBMA, 12 SBMA, and 33% w/w SBMA and with respect to PVAGMA shows that the size of the elastic hysteresis is least in the hydrogel sample composed of 100%w/w PVAGMA. In addition, the displacement of each cycle graph downward from the first curve shows the reduction in the elasticity of the hydrogel with each cycle. This is different for the curve of samples containing 33 and 12% w/w of SBMA respectively. The darkening of the curve for hydrogel PM88-SM12 represents a very slight displacement in each cyclic curve over 10 cycles. This darkening is not visible in the curve for the PM67-SM33 hydrogel. This observation may translate to the contributions of SBMA to the degree of elasticity. The recorded mechanical strengths determined in this study more than matched those obtained for PVA hydrogels reinforced with carboxylated nanocellulose whiskers.[9]

Table 3 outlines the derived parameters from the stress−strain compression curve of selected samples. There was an initial reduction in the compressive strength of PVAGMA hydrogel with the addition of SBMA (12%). The compressive strength subsequently increased with the increasing content of SBMA up to a limit. Similarly, Young's modulus, which measures a material's elasticity and response to applied force, increased with increasing content of SBMA. These results are comparative to results of previous studies that used hydroxyapatite for reinforcement and in which a peak stress of 2.3 MPa at 90% compression strain was recorded.[15] Though the highest peak stress in this study, 1.2 MPa, is lower than the 2.3 MPa recorded by Zhou and colleagues, these values may still be comparable considering that hydroxyapatite was used at 40% w/w for mechanical reinforcement before such a value could be obtained. Moreover, SBMA used in this study is considered a mechanically nonrobust polymer and was not anticipated to contribute to the mechanical robustness of the composite hydrogel in the manner it did.

The ElastosensBio, an instrument that employs laser light to nondestructively explore the transitions in the microstructure of a sample, was used to study the viscoelastic properties of the hydrogels over a temperature range of 25 to 37 °C to represent transitions between the room and the body temperatures, respectively. At each of these temperatures, the interplay between the shear storage modulus, shear loss modulus, G'', shear complex modulus, G^*, and tan d for each of the hydrogels is shown in Figure 3. The shear complex modulus defines the viscoelastic behavior of the hydrogels and represents the degree of elasticity with respect to the viscosity of the polymer chain properties.

https://doi.org/10.1021/acsomega.4c00228
ACS Omega 2024, 9, 31410−31426

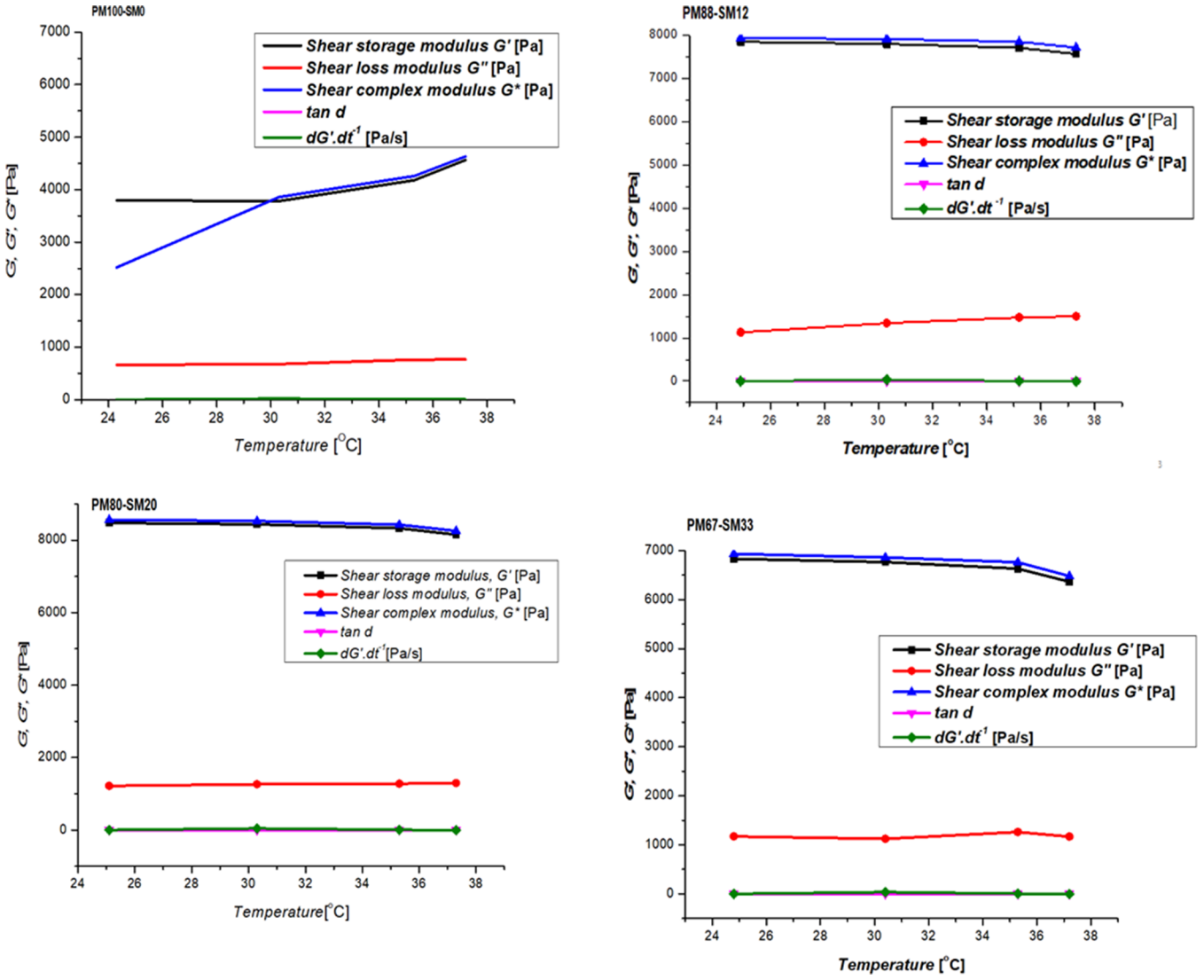

Figure 3. Graphical illustration of the G', G'', G^*, and tan d of hydrogels PM100-SM0, PM88-SM12, PM80-SM20, and PM67-SM33.

Above and below 20% w/w SBMA, the viscoelastic properties declined as was observed for the mechanical properties. The shear complex modulus for hydrogel PM100-SM0 increased stepwise with an increase in temperature, while the reverse was the case for other hydrogels containing SBMA. This may be an indication that SBMA contributes to a temperature-dependent effect.

The storage modulus of a polymer is a measure of the stiffness or solid-like properties of a polymer and represents the amount of energy input required to disrupt the solid structure. Shear loss modulus, conversely, is a measure of the liquid-like property of a polymer. When the G' is higher than the G'' in a polymer, it means that the polymer exists in a stiff or solid-like state. G' was higher than G'' for all hydrogel samples showing the stiff nature of the hydrogels. For PM100-SM0 containing only PVAGMA, the G' was lowest and increased slightly from 4 to 4.5 Kpa in going from 25 to 37 °C respectively. For the samples containing SBMA, the G' increased as the percentage of SBMA increased from 0 to 20% and afterward decreased. In addition, there was a negligible decrease in the G', contrary to what was seen in the PVAGMA hydrogel, for all samples containing SBMA as the temperature increased to 37 °C. This decrease was the least in the hydrogel sample with the highest G', PM80-SM20. In like manner, tan d, also known as damping, which is a measure of the energy dissipating ability of a material, varied across the hydrogels. In compression tests, tan d is derived from the area enclosed by the loading and unloading curve. Figure S5 shows the graph analyzing the damping potential of the hydrogels across different temperatures. Hydrogel PM88-SM12 noticeably had the best damping potential, even though it had the least compressive strength, while hydrogel PM80-SM20 which had the highest shear storage modulus and compressive strength showed the least capacity for damping. This observation is in line with the narration that two materials with the same shear storage modulus may have different capacities for damping. The shear storage modulus, G', which is a measure of the elasticity or solidity of the hydrogels, varied in a manner similar to the shear complex modulus across the formulations. As noted earlier, PM80-SM20 has the highest value of shear modulus 8.48 ± 0.93 kPa. In sample PM100-SM0 containing only PVAGMA, the shear storage modulus increased with temperature, contrary to what was observed for other samples. This means that the samples stiffened as the temperature approached body temperature. This observation may be particularly important as the compatibility of any biomaterial

https://doi.org/10.1021/acsomega.4c00228
ACS Omega 2024, 9, 31410−31426

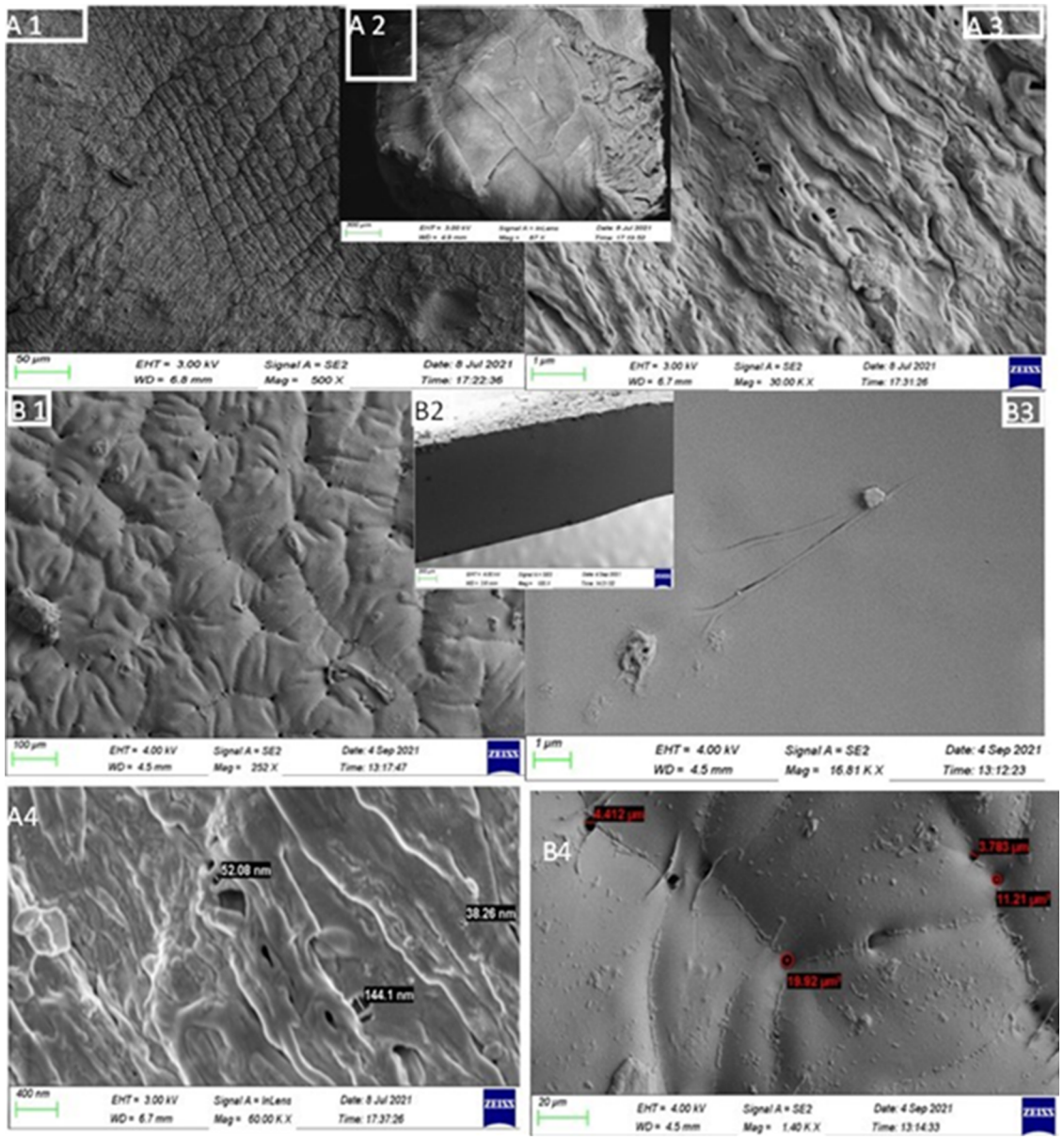

Figure 4. Scanning electron micrographs depicting the morphology of the planar and cross-sectional surfaces of dried hydrogels: (A1−4) with SBMA and (B1−4) without SBMA.

with body tissues depends very much on the stiffness or softness of the material under use conditions. All other samples became softer with an increase in temperature, though the decrease in the shear storage modulus was not as dramatic as that observed for hydrogel PM100-SM0.

Surface Morphology and Characterization. The scanning electron micrographs showing the surface morphology of planar and cross sections of hydrogel samples freeze fractured in liquid nitrogen are shown in Figure 4. Various morphologies have been reported for PVAGMA hydrogel samples cross-linked with different cross-linkers. Zhang and co-workers prepared PVAGMA hydrogels (with and without cellulose nanofibrils) using a photoinitiator.[13] They reported a densely porous morphology for all of the lyophilized hydrogel samples. Zhou and co-workers, on the other hand, while working on similarly prepared PVAGMA hydrogels (prepared with photoinitiators) but containing hydroxyapatite nanoparticles reported a dense nonporous morphology which they attributed to the collapse of the hydrogel structure occasioned by lyophilization.[15] The surfaces of the hydrogels in this study displayed dimpled and rough surfaces with pore-like structures under the SEM. In Figure 4A (1−3) and B (1−3), the morphologies of the hydrogel sample containing SBMA and that without SBMA are respectively shown at different magnifications while A4 and B4 captured the different pore sizes occurring in the hydrogel sample with SBMA and without SBMA respectively measured by the SEM. In contrast to the observations of these, A4 and B4 captured the different pore sizes occurring in the hydrogel sample with SBMA and without SBMA, respectively, measured by the SEM. In contrast to the observations of these previous studies, the morphologies observed in this study were of dense rough layers interspersed with pores of nonuniform sizes. Morgacheva and co-workers discussed the effect of cross-linking temperature on the porosity of PVAGMA hydrogels.[21] In their work in which hydrogels were cross-linked with potassium persulfate and

https://doi.org/10.1021/acsomega.4c00228
ACS Omega 2024, 9, 31410−31426

ascorbic acid, freezing conditions yielded macroporous gels while room temperature yielded isotropic gels. The photo-initiated cross-linking process may have contributed to the variability in the pore sizes encountered in this study. The nature of the pores encountered in hydrogels has been reported to contribute to the swelling. These may have additional implications for the fast release of medicaments incorporated into such hydrogels. The presence of nanosized pores may hinder the rapid release of enclosed medicaments, particularly as it is known that many hydrogels release their medication by swelling. According to the Wenzel model, the presence of nanostructures or surface roughness can contribute to the degree of hydrophilicity or hydrophobicity of a hydrophilic or hydrophobic material, respectively.[18,22] These structures, presenting as troughs, may play a role in complementing the hydrophilicity imparted by the zwitterionic polymer and its consequent effect on protein adsorption.[23]

Water Contact Angle (WCA) and Hydrophilicity of Hydrogels. The water contact angle is a measure of the hydrophilicity of any material and its propensity to limit protein adhesion. The mean water contact angle of a sessile drop of distilled water on equilibrium swollen hydrogel samples is shown in Table 4. Though the mean values of the measurements showed a highly hydrophilic surface, the standard variations showed the polydisperse distribution of this hydrophilicity across each surface. This may be a result of the heterogeneity in the distribution of cross-links within the hydrogel (particularly common with UV cross-links) with areas of dense and sparse cross-links as reported by Eke and co-workers.[24] Though in their study, the cross-link distribution was related to the mechanical performance of the hydrogel, cross-link distribution can also be related to the hydrophilicity of the hydrogels. The variability in the WCA of some hydrogels (results not shown as this was part of the optimization process) suggested that the distribution of the modifying zwitterionic SBMA across the two surfaces may differ, contributing to this variability. It was posited that the open nature of the glass tube mold additionally contributed to this variability, hence an alternate mold consisting of two glass plates separated by a 0.75 mm spacer. The results obtained thereafter showed that both surfaces were superhydrophilic with a WCA below 10° for both surfaces. There was a progressive decrease in the water contact angles of the hydrogels as the concentration of SBMA increased as shown in Table 4. Additionally, the non-zwitterionized PM100-SM0 hydrogel had a very low WCA as a standalone hydrogel. The WCA has been used as a measure of the surface hydrophilicity of hydrogels which in turn depends on the chemistry of groups accumulating on the surface of the hydrogels.[25,26] The contributions of the zwitterionic SBMA to the hydrophilicity of the hydrogels arise from the nature of its interaction with water molecules via ionic solvation. It is hypothesized that this, in addition to the contributions of the interactions of PVAGMA with water through hydrogen bonding, resulted in superhydrophilicity. Goda and group had previously reported no dependency between the WCA and water content.[27]

Table 4. Water Contact Angle of Sample Hydrogels

sample	water contact angle (deg)
PM100-SM0	27.7 ± 6.6
PM88-SM12	15.8 ± 5.9
PM80-SM20	13.7 ± 6.9
PM67-SM33	9.8 ± 1.0

Equilibrium Water Uptake (EWU) of the Hydrogels. The very high application rate of hydrogels in biomedical fields derives partly from their high water content, which makes

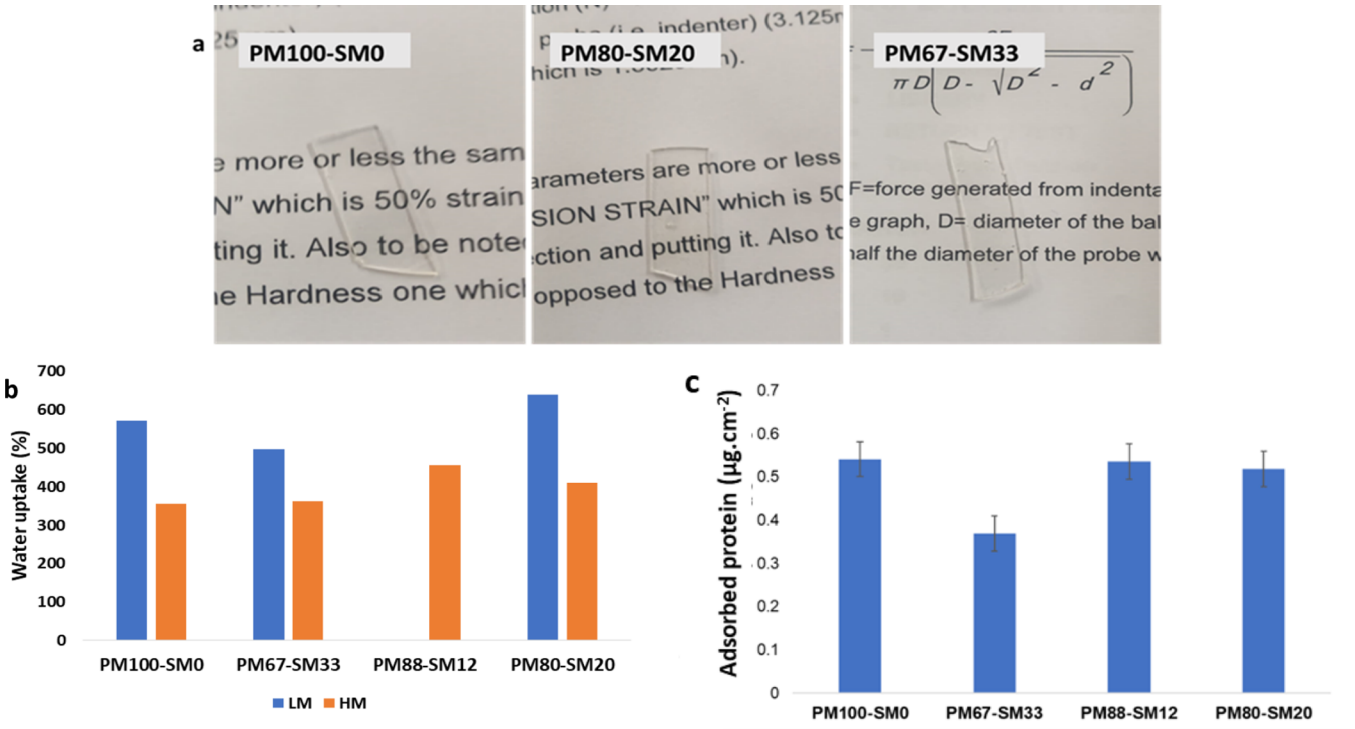

Figure 5. (a) Digital images of equilibrium swollen hydrogels, (b) water uptake (%) as a function of degree of methacrylation, and (c) protein adsorption by hydrogels.

https://doi.org/10.1021/acsomega.4c00228
ACS Omega 2024, 9, 31410−31426

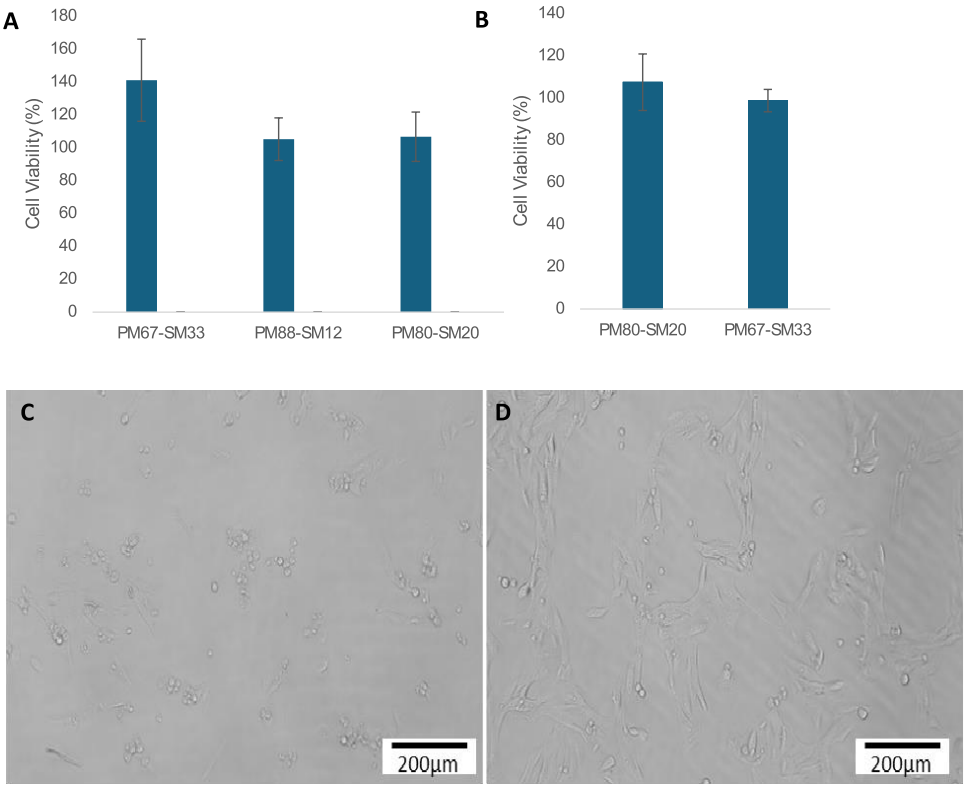

Figure 6. Viabilities (%) of (A) 3T3 and (B) HREP cells at 24 h in the presence of the hydrogel systems. Microscopic images depicting morphology of HREP cells treated with (C) ATF and (D) hydrogel extract at 48 h (scale bar = 200 μm).

them resemble biological environments. In addition, the rate and extent of swelling in hydrogels underpin certain abilities of their to act as drug delivery platforms. In ocular applications such as contact lenses, high water content is additionally desirable since high water content translates to oxygen permeability, which is a core requirement for corneal health in such applications. The digital images of some water-swollen hydrogel samples are shown in Figure 5a, while the results of the EWU of the samples are represented in Figure 5b. Percent swelling was observed to depend on the degree of methacrylation of the PVAGMA, its concentration, and the concentration of the cross-linking agent. Previous studies have reported the rapid and high swelling capacity of PVAGMA hydrogels.[15,28] Results shown in Figure 5b confirm that as the degree of methacrylation increased, the degree of swelling reduced. Inclusion of SBMA increased the degree of swelling for all hydrogel samples up to a limit. Beyond 20% w/w content of SBMA, the percent swelling decreased. This observation may be connected to the presence of structured water around the zwitterionic group of SBMA. Some other researchers also made a similar observation about a different zwitterionic polymer, 2 methacryloyloxyethylphosphorylcholine.[7,27] At all concentrations, the degree of swelling was higher in hydrogels with PVGMA with higher methacrylation (HM). This is expected since higher methacrylation would result in higher cross-linking density and reduced swelling. The degree of swelling is a very good index of the equilibrium water content in hydrogels. It also correlates well with the oxygen permeability in hydrogels for ocular application. In hydrogels designed for contact lens applications, it has been reported that the oxygen permeability increases with the equilibrium water content of the hydrogel. In such applications, swelling becomes an important index in establishing the ability of the cornea to become oxygenated while the contact lens is worn. In this context, the hydrogels from this study outperformed many hydrogels from regular contact lens polymers.

In addition, it is expected that the mechanical robustness of hydrogels will decrease with high water content. It was interesting to note that the mechanical robustness of the prepared hydrogels was not compromised (at least within the possible potential ocular uses) with the very high water content as was observed in some other hydrogels when water content is high.[27]

Protein Adsorption onto the PVAGMA Hydrogel Samples. Within minutes of contact with biological fluids, proteins, and lipids adsorb onto the implant material. For ocular devices such as contact and intraocular lens, the initial protein adsorption may lead to opacification, blurring, biofilm formation, pro-inflammatory response, consequent full-blown foreign body response, and even ultimate failure of the implant. Many attempts at limiting the initial protein adsorption for ocular biomaterials have predominantly involved surface modification with hydrophilic and zwitterionic polymers. The results obtained from protein adsorption studies are shown in Figure 5c. Previous studies have used single protein solutions in the determination of protein adhesion to biomaterials. Unfortunately, these do not adequately represent the complex protein components of biological systems. In this report, the calibration curve for the determination of adsorbed protein on the hydrogels was determined using an ATF composed of 3 major proteins found in tear fluid, lysozyme, bovine serum albumin (BSA), and mucin. Determination of the total protein adsorbed onto the hydrogel samples was subsequently evaluated using the same protein solution. The total adsorbed protein per unit area of the hydrogel disc across both pristine and zwitterionized hydrogels was below 0.6 μg/cm^2. Hydrogel

https://doi.org/10.1021/acsomega.4c00228
ACS Omega 2024, 9, 31410−31426

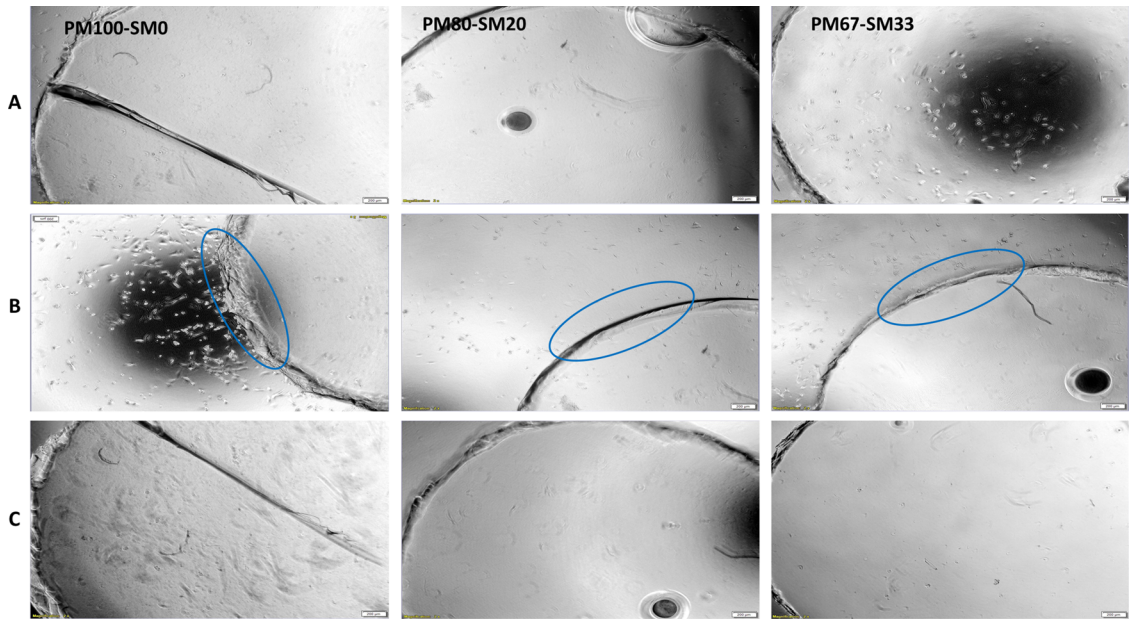

Figure 7. Microscopic images of (A) hydrogels in the presence of HREP cells (microscopic focus on hydrogels), (B) boundary between the hydrogel and plate in the presence of HREP cells (microscopic focus on the background), and (C) hydrogels following transference to fresh medium (scale bar = 200 μm; 2× magnification).

PM67-SM33 containing the highest amount of SBMA had the least protein adsorption (0.369 ± 0.077 $\mu g/cm^2$). Zwitterionization resulted in a statistically significant (at 90% confidence interval) reduction (31.70%) in the level of adsorbed protein when compared to the nonzwitterionized hydrogel (0.541 ± 0.002 $\mu g/cm^2$). The concentration of SBMA, however, did not contribute to a statistically significant difference when the protein adsorption capacity among the zwitterionized hydrogels was analyzed using one-way ANOVA at a 95% confidence interval. Different studies have reported the protein adsorption resistance properties of SBMA-modified materials. However, the reduction in protein adsorption reported in some of these previous studies approaches a 50% decrease when compared with the current study for all hydrogel samples. Zhang and colleagues reported protein adsorption of approximately 0.4 $\mu g/mL$ and 0.9 $\mu g/mL$, respectively, for BSA and lysozyme from single protein solutions using BCA assay kit.[29] The current study, however, studied protein adsorption from a mixed protein solution using a micro BCA assay kit that had a higher sensitivity. The protein adsorbed on the best-modified hydrogel sample was below the limit of detection by the micro-BCA assay kit and hence was calculated from the absorbance values using the equation generated from the standard curve of the protein solution. PVA has previously been used as a standalone agent for imparting hydrophilicity to materials.[30] In addition, certain already marketed contact lenses are composed of PVA as a base polymer, including already marketed products. Likewise, zwitterionic polymers such as 2-methacryloyioxyethyl phosphorylcholine have previously been used alone as a surface modifying agent to limit protein adsorption.[31,32] The results obtained imply a synergistic superhydrophilicity arising from the combination of PVA and the zwitterionic SBMA resulting in a higher capacity to limit protein adhesion in the developed biomaterial. Contrary to the traditional surface modification to which zwitterionics have previously been applied, SBMA was incorporated in the structure of the base PVAGMA polymer through a cross-linking process that potentially maintains the lifetime of the protein resistance of the developed material.

Cytotoxicity Assay of the Hydrogel Extract. The MTT assay has been employed as a relative tool to assess the toxicity of various compounds and materials on ocular cell lines. Primary human retinal epithelial cells were included in this study, as they represent the most sensitive, among ocular cells, to extraneous substances. Additionally, the International Organization for Standards (ISO) has outlined in vitro cell studies using applicable cell cultures and the requisite biomaterial extract as an acceptable means of initial biocompatibility assessment of the biomaterial and has been applied in related investigations for this purpose.[33,34] The results shown in Figure 6 represent the viabilities of (A) 3T3, (B) HREP, and (C, D) cells at 24 h in the presence of ATF and the hydrogel respectively. The cell viability in the presence of the positive control, ATF, was ∼100% for HREP. Although it has been noted that noncellular components may contribute to the optical density reading obtained in MTT assays and hence to very high viabilities in some instances,[35] effects of treatments can be corroborated by examining the morphology of the cells before treatment with MTT. The viabilities obtained here show generally the nontoxicity of the leached extract from the hydrogels across all cell lines used. The viabilities at 48 h were notably higher than the viabilities at 24 h across most cell lines for all the formulations, exceeding 100%. This could be due to the components of the hydrogel potentially either contributing to cell growth or metabolizing the MTT. Viabilities above 100%, as observed in this study, have resulted in the interrogation of the use of MTT as an assay method for assessing cytotoxicity in certain studies.[36] In this study, a repeat of the cytotoxicity assay employing methoxynitrosulfophenyltetrazolium carboxanilide (XTT) yielded similar toxicity profiles to MTT (results not included). The assertion of the effect of the hydrogel extract on the cells was collaboratively inferred from the visual inspection of the images of the cells treated with the leached hydrogel extract

https://doi.org/10.1021/acsomega.4c00228
ACS Omega 2024, 9, 31410−31426

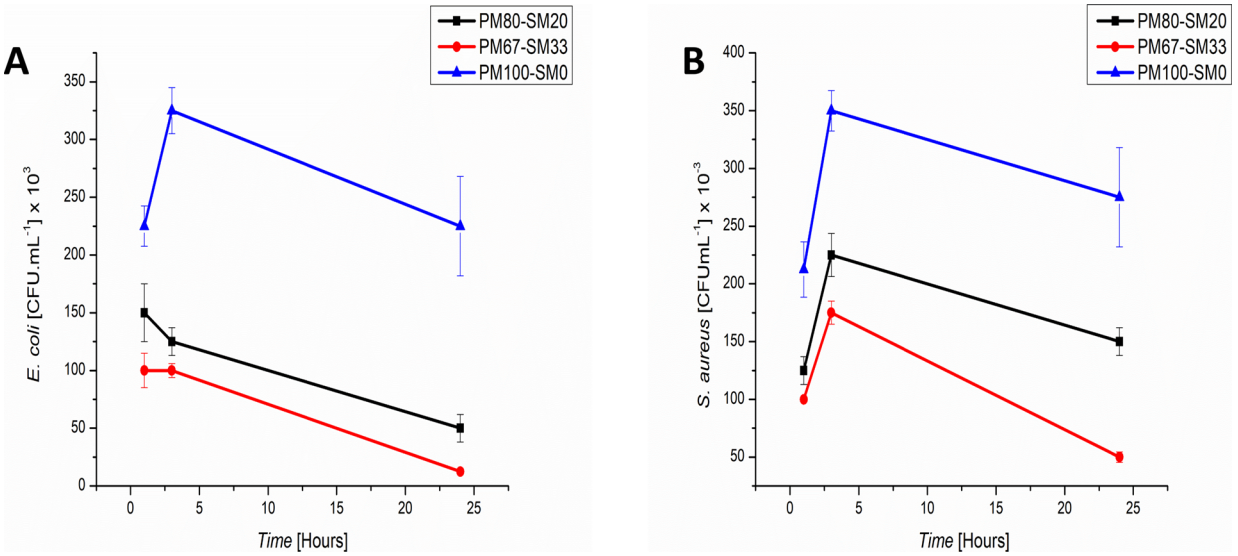

Figure 8. Number of *E. coli* (A) and *S. aureus* (B) cells adhering to the hydrogels.

and the positive control acquired just before the introduction of the MTT reagent. The results obtained at 48 h are not presented here due to cell viability already at acceptable levels at 24 h, and subsequent readings may be somewhat skewed.

In addition, the cell viabilities at all time points showed a graded response, with viabilities increasing proportionately to an increasing concentration of SBMA in the hydrogels across the 3T3 cell line. This effect may relate to the similarity of SBMA to membrane proteins, hence contributing to a biocompatible environment for the cells due to its presence in the hydrogels. Thus, the cell viability was high and exceeded 100% in some instances, indicating that the extracts may have had a proliferative effect on all of the cells. Other investigations assessing the in vitro biocompatibility of ocular systems via the MTT assay have furnished cell viability results in a similar range (80−130%), and dilution of extracts did not result in morphologic changes or reductions in cell growth.[37]

The morphology of HREP cells is captured in Figure 6C,D. It is known that the morphology of cells is an indication of the stress to which they are exposed under any given condition. The results obtained for the morphologies after treatment with ATF (Figure 6C) and the hydrogel extract (Figure 6D) indicate a normal morphology. A high mitotic index usually indicated by high viability demonstrates the ability of cells to repair after injury.[38] The implication may be pertinent in instances where the developed hydrogel is used in procedures that involve wound healing. It is important to note that a previous work on ocular hydrogel contact lenses recorded similar viabilities.[39] Overall, these results highlight the safety of the developed biomaterial for ocular cell lines.

HREP Cell Adhesion Studies. A major benefit that can accrue from limiting protein adhesion for an ocular implant such as an intraocular lens is the potential reduction in the extent of posterior and anterior capsular opacification that frequently results from migration and attachment of lens epithelial cells on the freshly implanted IOL. In addition, as mentioned in the previous section, excessive scarring that mars cataract surgery in children can be reduced using an IOL lens that seriously limits the adhesion of lens epithelial cells. Figure 7 shows the digital micrographs of hydrogel discs with distinct levels of the zwitterionic modifier, SBMA, onto which HREP (representing ocular epithelial cells) were seeded. Different layers/levels were focused on in the images, i.e., in Figure 7A, the hydrogel is focused on, whereas in Figure 7B, the background is focused on in the region of the boundary between the hydrogel and plate. In Figure 7C, the hydrogel is visualized after being transferred to a fresh medium for each hydrogel. The images of hydrogels stained with DAPI from the confocal laser microscope were not included because no fluorescence could be detected from any of the gels indicating the absence of cells on the hydrogels. The transparency of the hydrogels was so high that the cells that attached to the well plate under the hydrogel were visible through the hydrogel when observed under the microscope. This was inferred from observations while focusing the microscope. When the microscope was focused such that the cells attached to the well plate were in view, the cells observed through the hydrogels became obscured, whereas if the focus was obtained using the cells on the hydrogels, the cells on the well plate appeared blurred. In the images displayed in Figure 7A−C, cells were not visible on the hydrogels. Clarity improved after the hydrogel discs were transferred to a fresh medium, as can be seen from the images displayed in panel C of Figure 7. To confirm that the cells observed from the top of the hydrogels were on the well plate, a sample of the hydrogel, PM100-SM0, was cut with a blade halfway through the hydrogel. The digital image of the cut hydrogel obtained at higher magnification shows clearly that the cells were on the well plate, not on the hydrogel (panel B of Figure 7). Interestingly, there was no visible difference in the cell adhesion potential across the modified and unmodified hydrogel. This may be chronicling the hydrophilic potential of PVA, the base polymer in PVAGMA to limit cell adhesion as a standalone agent. Various studies involving zwitterionic compounds mainly focused on coating the surface of a base material such as polystyrene and gold,[40,41] with the zwitterionic agent through grafting from or grafting to polymerization techniques. Unfortunately, the stability of such surface modifications has been called into question particularly when used in dynamic environments. Ultralow epithelial cell adhesion potential displayed by the developed hydrogels is similar to if not better than that observed for such surface-modified substrates.[40] The ultralow

https://doi.org/10.1021/acsomega.4c00228
ACS Omega 2024, 9, 31410−31426

cell adhesion capacity of the zwitterionized hydrogels developed may highlight a role in corneal healing and a potential application in corneal bandages. Huang and colleagues equally explored this potential in a zwitterionic nanocomposite gel containing nanoclay for wound healing even though the ocular space was not their focus.[20]

Biofouling Resistance Assessment for Hydrogels. Biofilm formation associated with implantable devices and consequent sepsis continues to be a challenge motivating the search for biomaterials that will inherently limit it.[42,43] Biofilms usually result when microorganisms adhering to a surface secrete lipopolysaccharide and glycocalyx that ultimately form a shield within which they can grow and multiply, limiting access to external assaults, and causing antibiotic resistance.[44] Biofouling assessment was undertaken by a third party blind to the components and formulation process of the hydrogels. Results obtained from the assessment of resistance to biofilm formation showed a graded response that depended on the SBMA content of the hydrogels. Hydrogel PM67-SM33 containing the highest level of zwitterionic SBMA was at least 50% less susceptible to biofilm adhesion when compared to the pure PVAGMA hydrogel sample, PM100-SM0, at all the time points and across the 2 microbes used for the assessment. In addition, the reduction in bacteria colonies by the PM67-SM33 hydrogel between the 1 h time point and 24 h time point was over 87% when compared to the 100% PVAGMA hydrogel. Moreover, the standard deviation for all measurements involving PM67-SM33 hydrogel was very low especially when compared to the 100% PVAGMA hydrogel. Figure 8A,B shows the graph of the number of bacteria adhering to each hydrogel at every time point measured. All of the hydrogels showed a similar trend in the *S. aureus* medium. The number of colony-forming units (CFU) initially increased before decreasing, as the hydrogel surface environment was not favorable for continued adhesion. A two-way analysis of variance was used to determine the effect of time and the SBMA content of the hydrogels as 2 independent factors on the number of bacteria adhering to the hydrogels. With a *p-value* of 0.011 and an *F*-value of 10.31, and at a 95% confidence interval, the SBMA content of the hydrogels significantly affected the number of bacteria adhering to the gels. Studies on biofilm adhesion to materials other than hydrogels abound, but very few relate to hydrogels. Ishihara and colleagues[45] recently studied bacterial adhesion to silicone contact lenses surface-modified with 2-methacryloyloxyethyl phosphorylcholine. The bacterial adhesion observed in their study was on the order of 108 cells. Likewise, Wang and colleagues studied the bacterial adhesion to a carboxybetaine and sulfobetaine-modified poly (ethylene terephthalate).[46] The number of CFU cells found on their best-modified surface was of the order of 10^6. These are orders of magnitude higher than that observed in this study. A synergistic relationship arose from the combination of PVA and the zwitterionic SBMA that resulted in this level of biofilm reduction. Biofouling is often preceded by protein adsorption. The presence of a biomaterial in any tissue is a very strong stimulus for the influx of blood and other body fluids that serve as sources of protein that are adsorbed onto the material.[47] Dosler and colleagues evaluated the efficacy of contact lens solutions vis-à-vis the contact lens materials and found that the presence of proteins such as lysozyme and albumin contributed to more biofilm adhesion as well as low water content.[48] It can therefore be stated that fouling is always preceded by the adsorption of proteins onto the biomaterial depending on the biomaterial properties. These adsorbed proteins further serve as a template for biofilm adhesion. These processes are hindered when the biomaterial being evaluated possesses characteristics such as high water content and resists protein adsorption. The sensitive nature of the ocular environment places an even higher standard on implants designed for ocular application.[49] Ocular devices such as contact lenses are constantly removed and replaced on the eye and hence require constant soaking in multipurpose lens cleaning solutions to remove adhering bacteria and lipids that may cause sight-threatening infections such as keratitis. The success of such a cleaning process depends on the duration of soaking, the type of adhering microbe, and the type of cleaning solution.[50] Studies have shown that in certain instances, cleaning solutions used for the duration of time stipulated by the manufacturer do not remove certain bacteria such as *Pseudomonas aeruginosa*.[51,52] In addition, the possible sudden emergence of superbugs and multidrug resistance among contact lens-adhering microbes could be complicating these issues for contact lens users.

CONCLUSIONS

This investigation outlined the facile synthesis of a PVAGMA hydrogel modified by a photo-cross-linking polymerization with SBMA under the influence of UV light. Physicochemical characterization confirmed the synthesis and chemical stability of PVAGMA from PVA and GMA. Progressing beyond surface modification and overcoming impediments to efficient copolymerization of zwitterionics with regular cross-linkers, in this investigation the zwitterionic SBMA was incorporated as an integral part of the ocular hydrogel. The properties of the synthesized hydrogel, in terms of mechanical strength, swelling, hydrophilicity, and transparency, were robust. The prepared hydrogel, by virtue of its hydrophilicity, morphology, and mechanical properties, additionally had a limiting effect on the protein resistance ability of the hydrogel and invariably on its antifouling potential.

ASSOCIATED CONTENT

Supporting Information

The Supporting Information is available free of charge at https://pubs.acs.org/doi/10.1021/acsomega.4c00228.

^{1}H NMR of pristine PVA and methacrylated PVA; ^{1}H NMR single methacrylation and double methacrylation; DSC thermogram of the SBMA monomer; DSC thermograms of PVAGMA hydrogels with different SBMA contents; TGA weight derivative of PVA, PVAGMA, and the hydrogels; and damping potential of sample hydrogels (PDF)

AUTHOR INFORMATION

Corresponding Author

Yahya E. Choonara − *Wits Advanced Drug Delivery Platform Research Unit, School of Therapeutic Sciences, Faculty of Health Sciences, University of the Witwatersrand, Johannesburg 2193, South Africa;* orcid.org/0000-0002-3889-1529; Email: yahya.choonara@wits.ac.za

Authors

Onyinye J. Uwaezuoke − *Wits Advanced Drug Delivery Platform Research Unit, School of Therapeutic Sciences, Faculty of Health Sciences, University of the Witwatersrand,*

https://doi.org/10.1021/acsomega.4c00228
ACS Omega 2024, 9, 31410−31426

Johannesburg 2193, South Africa; Present Address: Department of Pharmaceutics, Faculty of Pharmacy, Olabisi Onabanjo University, Ago-Iwoye, Ogun State, Nigeria; orcid.org/0000-0001-7490-3868

Pradeep Kumar − *Wits Advanced Drug Delivery Platform Research Unit, School of Therapeutic Sciences, Faculty of Health Sciences, University of the Witwatersrand, Johannesburg 2193, South Africa;* orcid.org/0000-0002-8640-4350

Lisa C. du Toit − *Wits Advanced Drug Delivery Platform Research Unit, School of Therapeutic Sciences, Faculty of Health Sciences, University of the Witwatersrand, Johannesburg 2193, South Africa*

Naseer Ally − *Department of Neurosciences, Division of Ophthalmology, University of the Witwatersrand, Johannesburg 2193, South Africa*

Complete contact information is available at: https://pubs.acs.org/10.1021/acsomega.4c00228

Author Contributions

The manuscript was written through contributions of all authors. All authors have given approval to the final version of the manuscript.

Funding

This research was supported by the National Research Foundation of South Africa (NRF).

Notes

The authors declare no competing financial interest.

■ ACKNOWLEDGMENTS

We acknowledge the Chemistry department of the University of Johannesburg, South Africa, for assistance with contact angle measurements.

■ ABBREVIATIONS

PEGDMA	polyethylene glycol dimetahcrylate
PVAGMA	poly(vinyl alcohol) glycidyl methacrylate
GMA	glycidyl mmethacrylate
SBMA	sulfobetaine methacrylate
DM	degree of methacrylatrion
HREP	human retinal epithelial cells
CNF	cellulose nanofibrils
ATF	artificial tear fluid

■ REFERENCES

(1) Huszank, R.; Szilágyi, E.; Szoboszlai, Z.; Szikszai, Z. Investigation of Chemical Changes in PMMA Induced by 1.6 MeV He+ Irradiation by Ion Beam Analytical Methods (RBS-ERDA) and Infrared Spectroscopy (ATR-FTIR). *Nucl. Instrum. Methods Phys. Res. Sect. B Beam Interact. Mater. At.* **2019**, *450*, 364−368.

(2) Caló, E.; Khutoryanskiy, V. V. Biomedical Applications of Hydrogels: A Review of Patents and Commercial Products. *Eur. Polym. J.* **2015**, *65*, 252−267.

(3) Baino, F.; Potestio, I. Orbital Implants: State-of-the-Art Review with Emphasis on Biomaterials and Recent Advances. *Mater. Sci. Eng., C* **2016**, *69*, 1410−1428.

(4) Kharazmi, A.; Faraji, N.; Mat Hussin, R.; Saion, E.; Yunus, W. M. M.; Behzad, K. Structural, Optical, Opto-Thermal and Thermal Properties of ZnS-PVA Nanofluids Synthesized through a Radiolytic Approach. *Beilstein J. Nanotechnol.* **2015**, *6*, 529−536.

(5) Zhou, Y.; Dong, P.; Wei, Y.; Qian, J.; Hua, D. Synthesis of Poly(Sulfobetaine Methacrylate)-Grafted Chitosan under γ-Ray Irradiation for Alamethicin Assembly. *Colloids Surf. B Biointerfaces* **2015**, *132*, 132−137.

(6) Lalani, R.; Liu, L. Synthesis, Characterization, and Electrospinning of Zwitterionic Poly(Sulfobetaine Methacrylate). *Polymer* **2011**, *52* (23), 5344−5354.

(7) Carr, L. R.; Xue, H.; Jiang, S. Functionalizable and Nonfouling Zwitterionic Carboxybetaine Hydrogels with a Carboxybetaine Dimethacrylate Crosslinker. *Biomaterials* **2011**, *32* (4), 961−968.

(8) Kita, M.; Ogura, Y.; Honda, Y.; Hyon, S.-H.; Cha, W.-I.; Ikada, Y. Evaluation of Polyvinyl Alcohol Hydrogel as a Soft Contact Lens Material. *Graefes Arch. Clin. Exp. Ophthalmol.* **1990**, *228* (6), 533−537.

(9) Tummala, G. K.; Joffre, T.; Lopes, V. R.; Liszka, A.; Buznyk, O.; Ferraz, N.; Persson, C.; Griffith, M.; Mihranyan, A. Hyperelastic Nanocellulose-Reinforced Hydrogel of High Water Content for Ophthalmic Applications. *ACS Biomater. Sci. Eng.* **2016**, *2* (11), 2072−2079.

(10) Fathi, E.; Atyabi, N.; Imani, M.; Alinejad, Z. Physically Crosslinked Polyvinyl Alcohol−Dextran Blend Xerogels: Morphology and Thermal Behavior. *Carbohydr. Polym.* **2011**, *84* (1), 145−152.

(11) Strawhecker, K. E.; Manias, E. Structure and Properties of Poly(Vinyl Alcohol)/Na+ Montmorillonite Nanocomposites. *Chem. Mater.* **2000**, *12* (10), 2943−2949.

(12) Xiang, T.; Lu, T.; Xie, Y.; Zhao, W.-F.; Sun, S.-D.; Zhao, C.-S. Zwitterionic Polymer Functionalization of Polysulfone Membrane with Improved Antifouling Property and Blood Compatibility by Combination of ATRP and Click Chemistry. *Acta Biomater.* **2016**, *40*, 162−171.

(13) Zhang, J.; Liu, T.; Liu, Z.; Wang, Q. Facile Fabrication of Tough Photocrosslinked Polyvinyl Alcohol Hydrogels with Cellulose Nanofibrils Reinforcement. *Polymer* **2019**, *173*, 103−109.

(14) PubMed Entry. http://www.ncbi.nlm.nih.gov/pubmed/25821695 (accessed September 11, 2021).

(15) Zhou, D.; Dong, Q.; Liang, K.; Xu, W.; Zhou, Y.; Xiao, P. Photocrosslinked Methacrylated Poly(Vinyl Alcohol)/Hydroxyapatite Nanocomposite Hydrogels with Enhanced Mechanical Strength and Cell Adhesion. *J. Polym. Sci. Part Polym. Chem.* **2019**, *57* (18), 1882−1889.

(16) Yang, C.-C.; Wu, G. M. Study of Microporous PVA/PVC Composite Polymer Membrane and It Application to MnO2 Capacitors. *Mater. Chem. Phys.* **2009**, *114* (2), 948−955.

(17) Muniz, F. T. L.; Miranda, M. a. R.; Morilla Dos Santos, C.; Sasaki, J. M. The Scherrer Equation and the Dynamical Theory of X-Ray Diffraction. *Acta Crystallogr. Sect. Found. Adv.* **2016**, *72* (3), 385−390.

(18) El-Shamy, A. G.; Attia, W.; Abd El-Kader, K. M. The Optical and Mechanical Properties of PVA-Ag Nanocomposite Films. *J. Alloys Compd.* **2014**, *590*, 309−312.

(19) Crispim, E. G.; Piai, J. F.; Fajardo, A. R.; Ramos, É. R.; Nakamura, T. U.; Nakamura, C.; Rubira, A. F.; Muniz, E. Hydrogels Based on Chemically Modified Poly(Vinyl Alcohol) (PVA-GMA) and PVA-GMA/Chondroitin Sulfate: Preparation and Characterization. *Express Polym. Lett.* **2012**, *6*, 383−395, DOI: 10.3144/EXPRESSPOLYMLETT.2012.41.

(20) Huang, K.-T.; Fang, Y.-L.; Hsieh, P.-S.; Li, C.-C.; Dai, N.-T.; Huang, C.-J. Zwitterionic Nanocomposite Hydrogels as Effective Wound Dressings. *J. Mater. Chem. B* **2016**, *4* (23), 4206−4215.

(21) Morgacheva, A. A.; Artyukhov, A. A.; Panov, A. V.; Gordienko, M. G.; Shtilman, M. I.; Mezhuev Ya, O. Synthesis of Polyvinyl Alcohol with Methacrylate Groups and of Hydrogels Based on It. *Russ. J. Appl. Chem.* **2015**, *88* (4), 617−621.

(22) Ying, T.; Su, J.; Jiang, Y.; Ke, Q.; Xu, H. A Pre-Wetting Induced Superhydrophilic/Superlipophilic Micro-Patterned Electrospun Membrane with Self-Cleaning Property for on-Demand Emulsified Oily Wastewater Separation. *J. Hazard. Mater.* **2020**, *384*, No. 121475.

(23) Askari, F.; Zandi, M.; Shokrolahi, P.; Tabatabaei, M. H.; Hajirasoliha, E. Reduction in Protein Absorption on Ophthalmic Lenses by PEGDA Bulk Modification of Silicone Acrylate-Based Formulation. *Prog. Biomater.* **2019**, *8* (3), 169−183.

(24) Eke, G.; Mangir, N.; Hasirci, N.; MacNeil, S.; Hasirci, V. Development of a UV Crosslinked Biodegradable Hydrogel Containing Adipose Derived Stem Cells to Promote Vascularization for Skin Wounds and Tissue Engineering. *Biomaterials* **2017**, *129*, 188−198.
(25) Pop-Georgievski, O.; Rodriguez-Emmenegger, C.; Pereira, Santos; De Los, A.; Proks, V.; Brynda, E.; Rypáček, F. Biomimetic Non-Fouling Surfaces: Extending the Concepts. *J. Mater. Chem. B* **2013**, *1* (22), 2859−2867.
(26) Rostam, H. M.; Singh, S.; Salazar, F.; Magennis, P.; Hook, A.; Singh, T.; Vrana, N. E.; Alexander, M. R.; Ghaemmaghami, A. M. The Impact of Surface Chemistry Modification on Macrophage Polarisation. *Immunobiology* **2016**, *221* (11), 1237−1246.
(27) Goda, T.; Matsuno, R.; Konno, T.; Takai, M.; Ishihara, K. Protein Adsorption Resistance and Oxygen Permeability of Chemically Crosslinked Phospholipid Polymer Hydrogel for Ophthalmologic Biomaterials. *J. Biomed. Mater. Res., Part B* **2009**, *89* (1), 184−190.
(28) Cavalieri, F.; Miano, F.; D'Antona, P.; Paradossi, G. Study of Gelling Behavior of Poly(Vinyl Alcohol)-Methacrylate for Potential Utilizations in Tissue Replacement and Drug Delivery. *Biomacromolecules* **2004**, *5* (6), 2439−2446.
(29) Zhang, W.; Li, G.; Lin, Y.; Wang, L.; Wu, S. Preparation and Characterization of Protein-Resistant Hydrogels for Soft Contact Lens Applications via Radical Copolymerization Involving a Zwitterionic Sulfobetaine Comonomer. *J. Biomater. Sci. Polym. Ed.* **2017**, *28* (16), 1935−1949.
(30) Winterton, L. C.; Lally, J. M.; Sentell, K. B.; Chapoy, L. L. The Elution of Poly (Vinyl Alcohol) from a Contact Lens: The Realization of a Time Release Moisturizing Agent/Artificial Tear. *J. Biomed. Mater. Res. B Appl. Biomater.* **2007**, *80B* (2), 424−432.
(31) Goda, T.; Ishihara, K. Soft Contact Lens Biomaterials from Bioinspired Phospholipid Polymers. *Expert Rev. Med. Devices* **2006**, *3* (2), 167−174.
(32) Shi, X.; Cantu-Crouch, D.; Sharma, V.; Pruitt, J.; Yao, G.; Fukazawa, K.; Wu, J. Y.; Ishihara, K. Surface Characterization of a Silicone Hydrogel Contact Lens Having Bioinspired 2-Methacryloyloxyethyl Phosphorylcholine Polymer Layer in Hydrated State. *Colloids Surf. B Biointerfaces* **2021**, *199*, No. 111539.
(33) ISO 10993−5:2009(en), *Biological evaluation of medical devices—Part 5: Tests for in vitro cytotoxicity*. https://www.iso.org/obp/ui/#iso:std:iso:10993:-5:ed-3:v1:en (accessed February 25, 2024).
(34) Onuki, Y.; Bhardwaj, U.; Papadimitrakopoulos, F.; Burgess, D. J. A Review of the Biocompatibility of Implantable Devices: Current Challenges to Overcome Foreign Body Response. *J. Diabetes Sci. Technol.* **2008**, *2* (6), 1003−1015.
(35) Ghasemi, M.; Turnbull, T.; Sebastian, S.; Kempson, I. The MTT Assay: Utility, Limitations, Pitfalls, and Interpretation in Bulk and Single-Cell Analysis. *Int. J. Mol. Sci.* **2021**, *22* (23), No. 312827.
(36) Jaszczyszyn, A.; Gasiorowski, K. Limitations of the MTT Assay in Cell Viability Testing. *Adv. Clin. Exp. Med.* **2008**, *17* (5), 525−529.
(37) Bae, S. H.; Che, J. H.; Seo, J. M.; Jeong, J.; Kim, E. T.; Lee, S. W.; Koo, K. I.; Suaning, G. J.; Lovell, N. H.; Cho, D. I.; Kim, S. J.; Chung, H. In Vitro Biocompatibility of Various Polymer-Based Microelectrode Arrays for Retinal Prosthesis. *Invest. Ophthalmol. Vis. Sci.* **2012**, *53*, 2653−2657.
(38) Edelhauser, H. F. The Balance between Corneal Transparency and Edema The Proctor Lecture. *Invest. Ophthalmol. Vis. Sci.* **2006**, *47* (5), 1755−1767.
(39) Tran, N.-P.-D.; Ting, C.-C.; Lin, C.-H.; Yang, M.-C. A Novel Approach to Increase the Oxygen Permeability of Soft Contact Lenses by Incorporating Silica Sol. *Polymers* **2020**, *12* (9), 2087.
(40) Sobolčiak, P.; Popelka, A.; Mičušík, M.; Sláviková, M.; Krupa, I.; Mosnáček, J.; Tkáč, J.; Lacík, I.; Kasák, P. Photoimmobilization of Zwitterionic Polymers on Surfaces to Reduce Cell Adhesion. *J. Colloid Interface Sci.* **2017**, *500*, 294−303.
(41) Chou, Y.-N.; Sun, F.; Hung, H.-C.; Jain, P.; Sinclair, A.; Zhang, P.; Bai, T.; Chang, Y.; Wen, T.-C.; Yu, Q.; Jiang, S. Ultra-Low Fouling and High Antibody Loading Zwitterionic Hydrogel Coatings for Sensing and Detection in Complex Media. *Acta Biomater.* **2016**, *40*, 31−37.
(42) Jamal, M.; Ahmad, W.; Andleeb, S.; Jalil, F.; Imran, M.; Nawaz, M. A.; Hussain, T.; Ali, M.; Rafiq, M.; Kamil, M. A. Bacterial Biofilm and Associated Infections. *J. Chin. Med. Assoc.* **2018**, *81* (1), 7−11.
(43) Fujii, K.; Matsumoto, H. N.; Koyama, Y.; Iwasaki, Y.; Ishihara, K.; Takakuda, K. Prevention of Biofilm Formation with a Coating of 2-Methacryloyloxyethyl Phosphorylcholine Polymer. *J. Vet. Med. Sci.* **2008**, *70* (2), 167−173.
(44) Chew, S. C.; Yang, L.. Biofilms; In Caballero, B.; Finglas, P. M.; Toldrá, F., Eds.; *Encyclopedia of Food and Health*; Academic Press: Oxford, 2016, pp. 407−415. doi: DOI: 10.1016/B978-0-12-384947-2.00069-6.
(45) Ishihara, K.; Fukazawa, K.; Sharma, V.; Liang, S.; Shows, A.; Dunbar, D. C.; Zheng, Y.; Ge, J.; Zhang, S.; Hong, Y.; Shi, X.; Wu, J. Y. Antifouling Silicone Hydrogel Contact Lenses with a Bioinspired 2-Methacryloyloxyethyl Phosphorylcholine Polymer Surface. *ACS Omega* **2021**, *6* (10), 7058−7067.
(46) Wang, Y.; Shen, J.; Yuan, J. Design of Hemocompatible and Antifouling PET Sheets with Synergistic Zwitterionic Surfaces. *J. Colloid Interface Sci.* **2016**, *480*, 205−217.
(47) Bixler, Gregory D.; Bharat, Bhushan Biofouling: Lessons from Nature. *Philos. Trans. R. Soc., A* **2012**, *370* (1967), 2381−2417.
(48) Dosler, S.; Hacioglu, M.; Yilmaz, F. N.; Oyardi, O. Biofilm Modelling on the Contact Lenses and Comparison of the in Vitro Activities of Multipurpose Lens Solutions and Antibiotics. *PeerJ.* **2020**, *8*, No. e9419.
(49) Uwaezuoke, O. J.; Kumar, P.; Pillay, V.; Choonara, Y. E. Fouling in Ocular Devices: Implications for Drug Delivery, Bioactive Surface Immobilization, and Biomaterial Design. *Drug Delivery Transl. Res.* **2021**, *11*, 1903.
(50) McAnally, C.; Walters, R.; Campolo, A.; Harris, V.; King, J.; Thomas, M.; Gabriel, M. M.; Shannon, P.; Crary, M. Antimicrobial Efficacy of Contact Lens Solutions Assessed by ISO Standards. *Microorganisms* **2021**, *9* (10), 2173.
(51) Dantam, J.; Subbaraman, L. N.; Jones, L. Adhesion of Pseudomonas Aeruginosa, Achromobacter Xylosoxidans, Delftia Acidovorans, Stenotrophomonas Maltophilia to Contact Lenses under the Influence of an Artificial Tear Solution. *Biofouling* **2020**, *36* (1), 32−43.
(52) Bacteria survive longer in contact lens cleaning solution than previously thought, study shows; *ScienceDaily*, 2014. https://www.sciencedaily.com/releases/2014/04/140416190926.htm (accessed April 22, 2022).

https://doi.org/10.1021/acsomega.4c00228
ACS Omega 2024, 9, 31410−31426